Identification of Smoke and Sulfuric Acid Aerosol in SAGE III/ISS Extinction Spectra Following the 2019 Raikoke Eruption

Travis N. Knepp[1], Larry Thomason[1], Mahesh Kovilakam[2,1], Jason Tackett[1], Jayanta Kar[2,1], Robert Damadeo[1], and David Flittner[1]

[1]NASA Langley Research Center, Hampton, Virginia 23681, USA
[2]Science Systems and Applications, Inc. Hampton, Virginia 23666, USA

Correspondence: Travis N. Knepp (travis.n.knepp@nasa.gov)

Abstract. The 2019 eruption of Raikoke was the largest volcanic eruption since 2011 and it was coincident with 2 major wildfires in the northern hemisphere. The impact of these events was manifest in the SAGE III/ISS extinction coefficient measurements. As the volcanic aerosol layers moved southward, a secondary peak emerged at an altitude higher than that which is expected for sulfuric acid aerosol. It was hypothesized that this secondary plume may contain a non-negligible amount of smoke contribution. We developed a technique to classify the composition of enhanced aerosol layers as either smoke or sulfuric acid aerosol. This method takes advantage of the different spectral properties of smoke and sulfuric acid aerosol, which is manifest in distinctly different spectral slopes in the SAGE III/ISS data. Herein we demonstrate the utility of this method using 4 case-study events (2018 Ambae eruption, 2019 Ulawun eruption, 2017 Canadian pyroCb, and 2020 Australian pyroCb) and provide corroborative data from the CALIOP instrument before applying it to the Raikoke plumes. We determined that, in the time period following the Raikoke eruption, smoke and sulfuric acid aerosol were present ~~throughout the atmosphere and the 2 aerosol types were preferentially partitioned to higher (smoke) and lower (sulfuric acid) altitudes~~ in the stratosphere, but found no conclusive support for smoke above 20 km. Herein, we present an evaluation of the performance of this classification scheme within the context of the aforementioned case-study events followed by a brief discussion of this method's applicability to other events, its limitations, as well as ~~its limitations~~ potential misclassifications.

1 Introduction

Located on the Kuril archipelago, Raikoke (48.3°N, 153.3°E) is a volcanic island that has a history of moderately-sized eruptions that have been recorded over the last 200 years (Tanakadate, 1925; Newhall and Self, 1982; Rashidov et al., 2019). The 22-June, 2019 eruption was the largest volcanic eruption since 2011 (Puyehue-Cordón Caulle) and injected ≈1.5 Tg of sulfur dioxide (SO_2) into the lower stratosphere (Muser et al., 2020; de Leeuw et al., 2021). While the Raikoke eruption is interesting by itself, the time period surrounding the eruption is of particular interest because of coincident ~~large wildfires in Russia and Canada~~ wildfires in the northern hemisphere (Kloss et al., 2021; Vaughan et al., 2021), resulting in ~~the presence of~~

both smoke and volcanically derived material being present in the northern hemisphere's (NH) lower stratosphere at the same time. To better appreciate the recondite synergistic significance of these events we have constructed this introduction in such a way as to inform the novice without distracting the cognoscenti. To this end, we will first put the magnitude of the Raikoke eruption into context with other eruptions followed by a brief discussion of the atmospheric impact of large wildfires. Finally, we will discuss the scientific interest of these coincident events for the current study and our motivation in conducting this study.

Stratospheric aerosol consists of submicron particles (Chagnon and Junge, 1961) that are composed primarily of sulfuric acid and water (Murphy et al., 1998) and play a crucial role in atmospheric chemistry and radiation transfer (Pitts and Thomason, 1993; Kremser et al., 2016; Wilka et al., 2018). Background stratospheric sulfuric acid is supplied by chronic, natural, emission of OCS (carbonyl sulfide), CS_2 (carbon disulfide), DMS (dimethyl sulfide), and SO_2 (sulfur dioxide), from both land and ocean sources (Kremser et al., 2016). The total amount of sulfur in the stratosphere is strongly modulated by volcanic activity. In the past few decades, this has most notably been the result of a few events like Pinatubo and El Chichón (McCormick et al., 1995). However, even relatively small events have been shown to impact stratospheric aerosol radiative forcing (Vernier et al., 2011), thus affecting climate and chemistry.

Volcanic eruptions have the potential to significantly change the atmosphere in several ways including changes in chemical composition, atmospheric dynamics, synoptic weather patterns, and radiation transfer. To facilitate comparison of volcanic events from a geological perspective, the Volcanic Explosivity Index (VEI) was developed by Newhall and Self (1982) and was later refined by Pyle (1995). While the VEI scale provides meaningful information for geologists (i.e., mass and volume of ejecta as well as rate of ejection), it retains little value for atmospheric scientists who are interested in what was ejected (e.g., SO_2, which is converted to sulfuric acid aerosol, as opposed to lava, rocks, and ash) and where the ejected material went (i.e., troposphere vs. stratosphere). However, the VEI scale remains in use by these scientists until a more meaningful scale is developed, ideally one that takes into consideration the climactic impact of these eruptions.

The VEI scale is based primarily on the volume of ejected tephra (solid material, not including gases) as described by Eq. 1 where V is the ejecta volume in cubic meters.

$$VEI = \log_{10}(V) - 4 \tag{1}$$

Therefore, for every integer step on the VEI scale the amount of ejecta increases by a factor of ten, making the largest eruptions (VEI >= 5) truly massive with ejecta volume on the order of cubic kilometers. To better appreciate the magnitude of the largest events the reader is encouraged to consider a few points: 1. the frequency of eruptions decreases approximately logarithmically as a function of VEI (VEI-7–8 occurring VEI-7 and VEI-8 occur every 1000–2000 years), 2. on average, eruptions of a given VEI eject ≈40% more ejecta than an eruption on rated at the next smaller VEI, 3. on average, eruptions with VEI-7 or VEI-8 are responsible for ≈50% of the total ejecta mass, ejecta volume, and thermal energy flux over the last 1000 years (Pyle, 1995).

The largest eruption within the last 500 years was the Mount Tambora eruption of 1815 (VEI-7), which released enough sulfur dioxide (SO_2), which was quickly converted to sulfuric acid aerosol in the stratosphere, to cool the northern hemisphere by up to 2 K. This resulted in the 1816 "year without summer" (Stothers, 1984; Schurer et al., 2019). Probably the

best known eruption in recent history is the 1991 eruption of Mount Pinatubo (VEI-6), which resulted in a global temperature ~~change of -1~~ reduction of 1 K and changed the stratospheric aerosol levels for 7–9 years (Deshler et al., 2003; Santer et al., 2014). Therefore, despite being relatively rare, large eruptions have a significant impact on short-term atmospheric
60   chemistry and physics. However, it is not *just* large eruptions that influence atmospheric chemistry and radiative transfer. On the contrary, it ~~has~~ been demonstrated that chronic eruptions of small volcanoes (VEI-3–4) play a measurable role as noted by Vernier et al. (2011), making them relevant to atmospheric chemistry and climate studies. While these eruptions lack the volume of their larger siblings, they make up for the difference in eruption frequency with VEI-3 eruptions taking place 4–5 times per year and VEI-4 eruptions occurring every 1-2 years. This results in a continual injection of SO_2,
65   and sometimes ash, into the lower stratosphere and free troposphere, sometimes with devastating consequences. ~~Possibly the most damaging eruption in this class was the Laki eruptions of 1783 (VEI-4) that consisted of both violent eruption events that resulted in plume heights of 15 km, and less-violent ejection of lava and gases that resulted in a volcanic fog (commonly referred to as vog). Continuing for 8 months, the Laki eruptions released a total of ≈120 Tg of SO_2, most of which remained within the troposphere (Thordarson and Self, 2003). To put this release of SO_2 in perspective, consider~~
70   ~~that the 1991 Pinatubo eruption (VEI-6) released only 20–30 Tg of SO_2 (Bluth et al., 1992; McCormick et al., 1995) and the 1815 eruption of Tambora (VEI-7) released ≈100 Tg of SO_2 (Pinto et al., 1989). Given the magnitude of SO_2 released, it is not surprising that the Laki eruption was responsible for the Icelandic "haze famine" wherein 20–25% of the Icelandic population died of starvation along with ≈60% of the grazing livestock (Thordarson and Self (1993, 2003) and references therein). This vog was also observed over England and Europe, possibly contributing to up to 20,000 additional deaths in~~
75   ~~England (Witham and Oppenheimer, 2004). While the loss of life has been attributed mainly to direct exposure to volcanic gases, it has been suggested that the stratospheric injections had significant climatological impact resulting in an unusually-cold winter throughout the entire northern hemisphere (Thordarson and Self, 2003). Though the extent of the climatological impacts have been called into question (D'Arrigo et al., 2011), the Laki eruptions serve as a prime example of how smaller eruptions can have significant impact on both life and climate.~~

80   Another source of stratospheric aerosol that has ~~become significant~~ received increasing attention over the past decade is large-scale, intense-burning, wildfire events that generate pyrocumulonimbus clouds (pyroCbs, also referred to as cumulonimbus flammagenitus), which were originally hypothesized to only exist as a product of nuclear explosions (Turco et al., 1983). These fires burn with sufficient intensity to form a cumulonimbus cloud and inject smoke and volatile organic compounds directly into the stratosphere (Fromm et al., 2006, 2010) on a scale comparable to a volcanic eruption of ~~VEI-3–4~~ VEI-3 or
85   VEI-4 (Peterson et al., 2018). The largest pyroCbs on record are the 2017 Canadian and 2020 Australian wildfires, both of which injected between 0.1 and 0.9 Tg of aerosol into the lower stratosphere (Peterson et al., 2018; Yu et al., 2019; Kablick III et al., 2020).

These biomass burning events release black and brown carbon aerosol ~~,~~ (BC and BrC, respectively), which is carried into the stratosphere. Unlike sulfuric acid aerosol, ~~black and brown carbon absorbs~~ BC and BrC absorb solar radiation causing it to heat
90   throughout the day. Due to this diabatic heating, the density of the air mass immediately around the particles decreases, thereby lofting the smoke plume to higher altitudes, well past the initial injection height and independent of the general atmospheric

circulation (Yu et al., 2019). This lofting effectively transports the chemical environment present in the lower atmosphere to higher altitudes, which can act as a tracer for pyroCb injections, as was demonstrated for the 2017 Canadian and 2019/2020 Australian wildfires ~~(Kablick III et al., 2020)~~(Boone et al., 2020; Kablick III et al., 2020). Further, displacing the background

95   stratospheric air with air that differs chemically and radiatively can also alter synoptic meteorology (Kablick III et al., 2020). Therefore, while pyroCbs lack the eruptive power of volcanic events, they have the potential to play a substantive role in short-term ground-level air quality (Johnston et al., 2020) as well as stratospheric chemistry and dynamics.

Given the broad impact of these two event types, and the fact that they influence the atmosphere in distinctly different ways, it is necessary to be able to distinguish between the two.

100   A ~~unique~~ combination of volcanic and pyroCb events occurred in 2019 when ~~the eruption of Raikoke was preceded by pyroCB events in Canada and Russia~~Raikoke erupted during the northern hemisphere's burn season. This coincidence presented both a scientific opportunity as well as measurement challenges. Raikoke injected SO_2 and ash to a peak altitude of $\approx$15 km (Thomason et al., 2021) ~~, resulting~~ with SO_2 detected shortly thereafter at 19 km (Hedelt et al., 2019). This resulted in an SO_2 column density in excess of 900 Dobson units (Hedelt et al., 2019) and an overall mass load of $\approx$1.5 Tg (Muser et al.,

105   2020; de Leeuw et al., 2021). This plume was transported to the northeast then down the western seaboard of North America before circling the globe (Hedelt et al., 2019; Chouza et al., 2020; Kloss et al., 2021; Vaughan et al., 2021). Herein we will show that part of the plume broke off from the ~~main~~ primary plume and continued to rise as it migrated equatorward, contrary to what has been previously observed for sulfuric acid aerosol, but is more typically associated with smoke. The working hypothesis ~~is~~ was that this secondary plume consisted, at least in part, of wildfire smoke. The question we sought to answer is whether a

110   positive identification of smoke in the secondary plume could be obtained using data from the Stratospheric Aerosol and Gas Experiment III aboard the International Space Station (SAGE III/ISS, hereafter referred to as SAGE). While other instruments such as the Ozone Mapping and Profiler Suite (OMPS), Atmospheric Chemistry Experiment Fourier-Transform Spectrometer (ACE-FTS), the Cloud-Aerosol Lidar with Orthogonal Polarization (CALIOP), and the Tropospheric Monitoring Instrument (TropOMI) are routinely used to observe wildfire and volcanic activity, it is important to understand the applicability of SAGE

115   data to these identifications. While coincident observations (in both time and space) strengthen the interpretation of each instrument's data, it is not always possible to have multiple instruments observe the same volume of the atmosphere within a reasonable time frame. Therefore, it is necessary to be able to understand the strengths and limitations of each individual instrument. To this end, we ~~present~~ evaluate a method of distinguishing between sulfuric acid aerosol and smoke in the stratosphere that uses the SAGE extinction spectra. We discuss limitations of this methodology, namely that it is limited to

120   moderately-sized eruptions (VEI $\leq$5) and large-scale pyroCb events as detailed below.

2   Instrumentation

2.1   SAGE III instrument and data preparation

SAGE is a solar and lunar occultation instrument (Cisewski et al., 2014) that is installed on the ISS and has a data record that began in June 2017. The spectrograph sub-system has a spectral range that extends from 280 to 1040 nm and has a resolution of

125   1-2 nm. In addition to the spectrograph there is an InGaAs photodiode at 1550 nm. The ISS orbit is inclined at 51.6°, resulting in more observations at midlatitudes than at tropical latitudes as shown by Knepp et al. (2020).

     The version 5.2 SAGE data were used in this analysis. The standard products include the number density of gas-phase species for both solar (O_3, NO_2, and H_2O) and lunar (O_3, NO_2, and NO_3) observations, as well as aerosol extinction coefficients (385, 450, 520, 600, 675, 755, 870, 1020, 1550 nm; referenced as k_λ) for solar occultations. The v5.2 release differed from v5.1

130   in that vertical smoothing for all products, except H_2O, was turned off to provide data at the highest vertical resolution. In this study, the extinction coefficients were filtered to remove data with relative errors in excess of 20% followed by vertical smoothing using a 1-2-1 binomial average to yield a vertical resolution consistent with previous SAGE missions (i.e., 0.75 km, reported every 0.5 km). Finally, the data were limited to altitudes between 2 km above the tropopause (as reported by the Modern-Era Retrospective analysis for Research and Applications, version 2 ~~(MERRA-2)~~ model) and 30 km.

135   The 520, 600, and 675 nm extinction coefficients had a low bias as demonstrated by Wang et al. (2020) for the v5.1 product, and this bias remains present in the v5.2 product. The bias is more prominent at mid-latitudes and altitudes between 20 and 25 km, and is likely the product of ozone interference in the retrieval algorithm. Therefore, k_{520} was replaced by applying an Ångström (power law) correction as described by Eq. (2) where ~~k~~ k is the extinction coefficient at the subscripted wavelength. The k_{520} channel was part of the original analysis code that was written for this study. However, it was later determined that

140   the analysis could have been carried out without the k_{520} channel with no impact on the interpretation of the results. Therefore, the correction method was included in this manuscript so the reader may understand how we initially intended to mitigate the impact of the low bias and to explain how the extinction coefficient data were prepared for use within the current study.

$$\log k_{520} = \frac{\log\left(\frac{k_{450}}{k_{755}}\right) \cdot \log\left(\frac{520}{755}\right)}{\log\left(\frac{450}{755}\right)} + \log k_{755} \tag{2}$$

2.2   CALIOP

145   The Cloud-Aerosol Lidar with Orthogonal Polarization (CALIOP) instrument is a space-borne elastic backscatter lidar that has been orbiting the earth in the A-train constellation since 2006 (Winker et al., 2010). In September 2018 the orbit was lowered by 16.5 km to correspond to the orbit of CloudSat~~which~~. The onboard Nd:YAG laser emits polarized radiation at 1064 nm and 532 nm. The total backscatter at 1064 nm and both parallel and perpendicular backscatter at 532 nm provides information on the size and shape of the scattering particles. We used data from the version 4.2 product (L1 for depolarization ratio and

150   L2 for the vertical feature masks), which has improved calibration particularly suitable for stratospheric studies (Kar et al., 2018; Getzewich et al., 2018; Kim et al., 2018). We also used the ~~level 3~~ L3 stratospheric aerosol product, which provides ~~aerosol extinction~~ monthly averaged aerosol extinction coefficients and attenuated scattering ratios (i.e., ratio of measured total attenuated backscatter to a modeled molecular backscatter; see Vaughan et al. (2009) for details) in the stratosphere at 5°(latitude), 20°(longitude), and 900 m (vertical) resolution (Kar et al., 2019).

155   ## 2.3   ACE-FTS

The Atmospheric Chemistry Experiment (ACE) is a space-borne instrument package that has been orbiting the earth since August, 2003. The primary instrument on ACE is a high-resolution (± 25 cm^{-1}) Fourier Transform Spectrometer (ACE-FTS) that collects solar spectra via the occultation technique (vertical resolution is ≈ 4 km Bernath et al. (2005), reported every 0.5 km). For instrument and algorithm details the reader is guided to Bernath et al. (2005) and Boone et al. (2005). While the ACE mission was designed to study, among other things, the impact that biomass burning events have on the troposphere, ACE-FTS data have been used to study the impact of pyroCbs on the lower stratosphere as well (Tereszchuk et al., 2013; Boone et al., 2020). Herein, the v4.2 ACE-FTS products were used to aid in identification of stratospheric smoke after the Raikoke eruption.

2.4 TropOMI

The Tropospheric Monitoring Instrument (TropOMI) is part of the European Space Agency's Sentinel-5 Precursor mission that is dedicated to monitoring air pollution from space and has been in orbit since October 2017. The instrument consists of a 2 dimensional spectrometer that yields a swath width of 2600 km, ground pixels sizes as good at 7 km x 3.5 km, and daily global coverage (Veefkind et al., 2012). The retrieval of SO_2 (v1.1, L2) is accomplished by using the spectrometer's third spectral band (310–405 nm; algorithm details can be seen in Theys et al. (2017)), which was used herein to identify the location of SO_2 plumes after the Raikoke eruption.

3 The Raikoke plumes

The 22-June, 2019 eruption of Raikoke was rated a VEI-4 that injected SO_2 and ash ~~directly~~ into the stratosphere~~(between 13 and~~, with SO_2 detected shortly thereafter at 19 km ~~)~~Hedelt et al. (2019). The SAGE instrument observed enhanced extinction layers within ~~one week~~ 10 days of the eruption ~~(as shown in~~ Fig. 1~~)~~. The immediate increase in extinction was $\approx$~~8-9~~ 9 times the background conditions, and the stratosphere remained in a non-background state throughout the remainder of 2019 and into ~~2020.~~ 2020 (Kloss et al., 2021). Figure 2 shows the monthly zonal mean extinction coefficient at 1550 nm (k_{1550}) and extinction ratio between the 520 nm and 1550 nm channels ($k_{520} : k_{1550}$) from SAGE as well as the attenuated scattering ratio from CALIOP. The progression of enhanced extinction is seen in panels a-f of Fig. 2. Beginning in July, the extinction coefficient increased between 11 and 13 km and is attributed to Raikoke. No significant enhancement was observed in June because these figures present monthly zonal means and the eruption occurred late in the month, effectively averaging out any enhancement that was detected in the SAGE data. Subsequent months showed significant enhancement as well as how this enhanced layer was transported southward, which is better seen in the extinction ratio plots (panels g-l) and attenuated scattering ratio from CALIOP (panels m-r).

What stood out in Fig. 2, panel (d), was the presence of an enhanced layer at ≈ 23 km. The initial ascent of this "secondary plume" might be seen as early as August (panel c) and remained visible in the extinction coefficient plots for the remainder of the year. The extinction ratio plots (panels g-r) as well as the attenuated scattering ratio plots (panels m-r) more readily show the persistence of this layer through November. Historically, extinction ratios have used the 1020 nm channel as reference. However, here we used the 1550 nm channel as reference because this ~~enhanced~~ accentuated the contrast between the enhanced

layers and background, resulting in a more prominent contrast. It is because of this heightened contrast that the 1550 nm channel was used for reference throughout the remainder of this analysis.

190   A possible reason for the lofting of this layer could be diabatic heating as has been demonstrated for smoke in previous wildfires (Boers et al., 2010; de Laat et al., 2012; Yu et al., 2019). Per this hypothesis, as the Sun shone through this portion of atmosphere, particles within the secondary plume absorbed the incoming solar radiation, which resulted in the air mass heating, thereby decreasing its density, which resulted in further lofting until equilibrium was reached. Though this scenario is not unreasonable for an absorbing aerosol, this is unexpected behavior for weakly-absorbing species like sulfuric acid aerosol

195 and is generally not observed in association with the mid and high-latitude eruptions of the past. Below 2 μm, the imaginary component of sulfuric acid's refractive index is effectively zero (i.e., $\ll$1E-5 ;-per Palmer and Williams (1975)), precluding the level of absorption required for subsequent heating/lofting. However, this behavior would be consistent with absorbing particles typically found in smoke from biomass burning events that occasionally inject ~~black and brown carbon~~ BC and BrC directly into the stratosphere during pyroCb events. Therefore, we hypothesized that smoke was present in the stratosphere

200 during the Raikoke eruption and that this smoke layer lofted up to ≈25 km as it circulated the globe and migrated southward as demonstrated in ~~Chouza et al. (2020)~~Chouza et al. (2020); Gorkavyi et al. (2021).

Observation of the Raikoke Plume on 2-July 2019
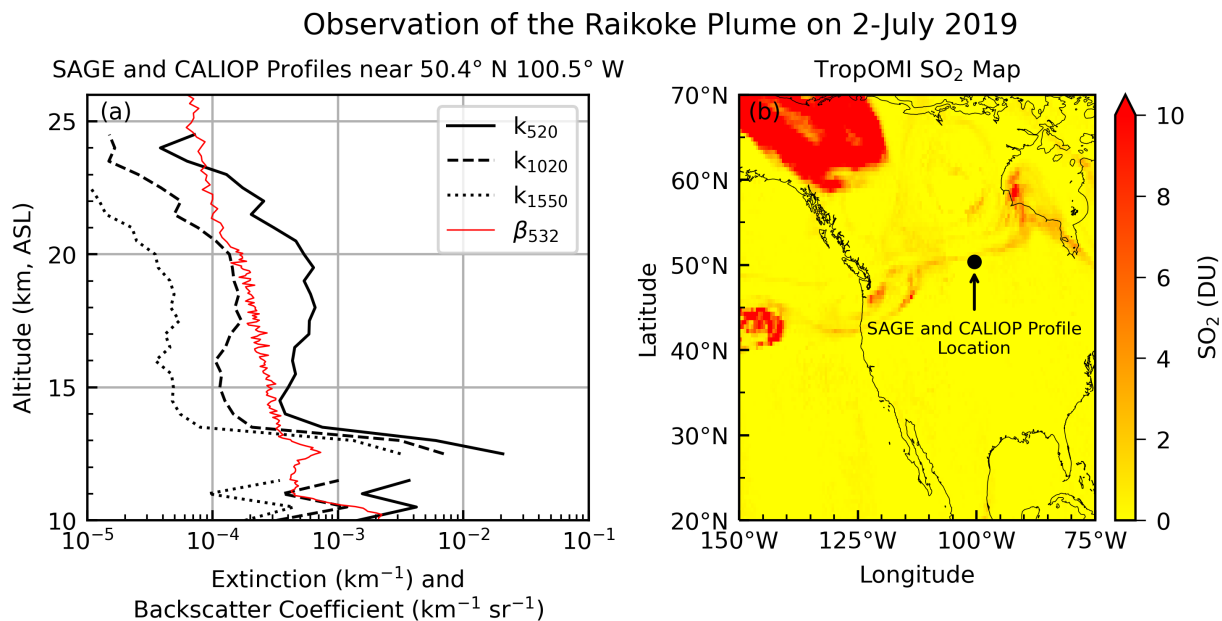
Figure 1. Observation of the Raikoke plume on 2-July 2019. SAGE extinction coefficient profiles at 3 wavelengths and CALIOP L1 backscatter profile showing the Raikoke plume between 12 and 14 km near 50.4° N and 100.5° W (panel a). Breaks in the SAGE profiles is where the algorithm failed to produce valid data. TropOMI SO$_2$ product showing a wisp of the SO$_2$ plume that intersected the SAGE and CALIOP fields of regard (panel b). The CALIOP granule used in this image was CAL_LID_L1-Standard-V4-10.2019-07-02T09-10-53ZN. The tropopause at this location was below 10 km.
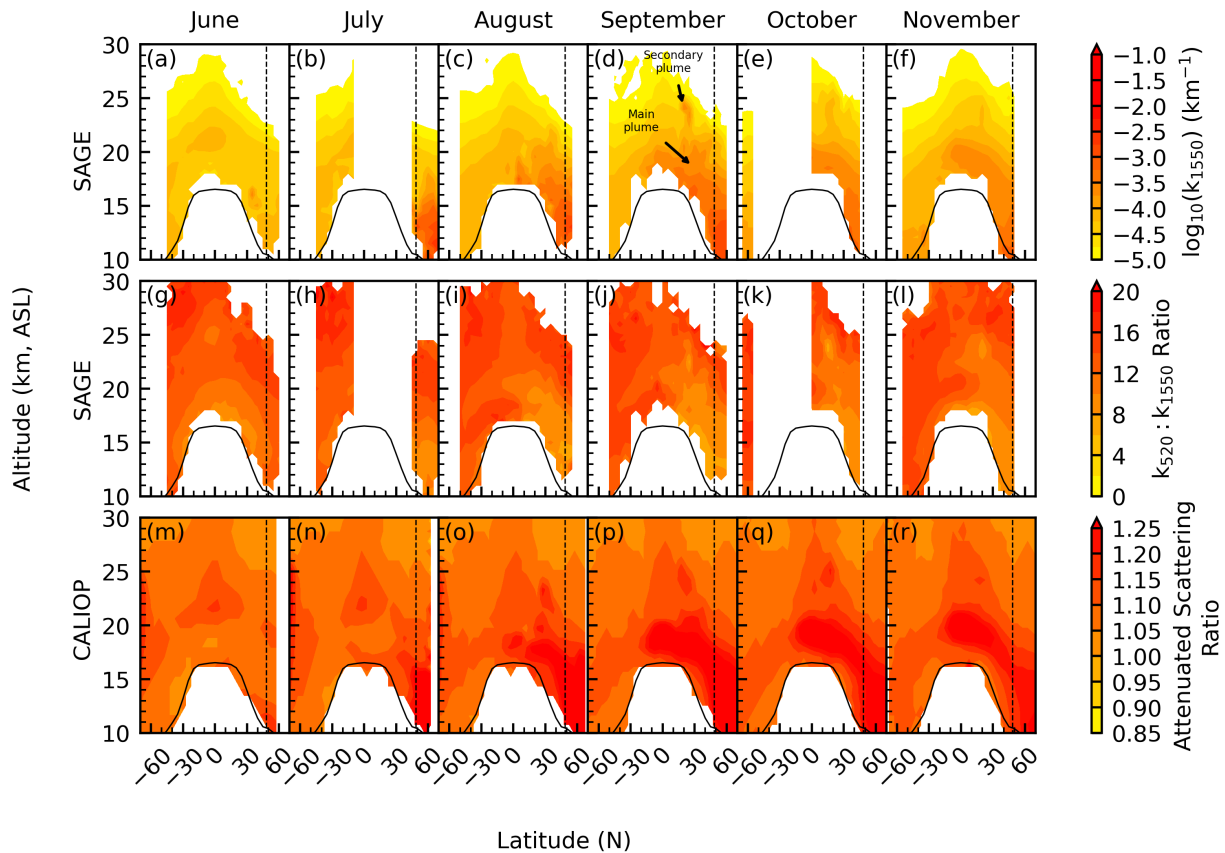
Figure 2. Zonal monthly mean of 1550 nm extinction coefficients (panels a-f), 520:1550 extinction ratio (panels g-l), and attenuated scattering ratio from CALIOP (panels m-r). The solid black line indicates the average tropopause altitude and the dashed black line indicates Raikoke's latitude.

4 Evaluation of smoke and sulfuric acid extinction spectra from Mie theory

In order for the ascending air mass to ~~be diabaticallyheated~~ heat diabatically, there must be an absorbing species present and we hypothesized that this absorbing species ~~is black and brown carbon~~ was BC and BrC found in smoke from ~~coincident wildfires in Siberia and western Canada~~ wildfires that occurred during the Raikoke time period. While the composition and spectral characteristics of smoke are highly variable ~~(Bergstrom et al., 2002; Müller et al., 2005; Park et al., 2018; Kozlov et al., 2014; Womack et al., 2~~ (Bergstrom et al., 2002; Müller et al., 2005; Park et al., 2018; Kozlov et al., 2014; Liu et al., 2015; Womack et al., 2021), there is commonality between burning events in that the real component of the refractive index is spectrally flat and the imaginary component is variable (both behaviors being significantly different from sulfuric acid aerosol). Therefore, it is reasonable that

the extinction spectra (extinction coefficients or extinction ratios as a function of wavelength) for smoke and sulfuric acid aerosols would differ significantly and that this difference may be useful in distinguishing between the two aerosol types.

As an initial test of this hypothesis we used Mie theory to calculate extinction coefficients at SAGE wavelengths for sulfuric acid aerosol and smoke. The primary challenge in carrying out this simulation is the highly-variable nature of smoke's refractive index, which is dependent on fuel source, burn conditions, age, etc. Further, smoke in the stratosphere is aged and its composition has likely changed during its transport by ongoing chemistry (Yu et al., 2019). Therefore, the likelihood of this smoke's refractive index being consistent with the refractive index measured within a laboratory setting or in situ measurements from an aircraft flying in the troposphere is small. To our knowledge there have been no composition or refractive index measurements for stratospheric smoke. Therefore, we used two sets of smoke refractive indices to span the range of reasonable refractive index values. The Bergstrom et al. (2002) refractive indices are representative of black carbon (BC) that comes from complete combustion, and the Sumlin et al. (2018) refractive indices are representative of brown carbon (BrC) smoke from biomass burning events (see Table 1 for values). While it is unlikely that stratospheric smoke is composed solely of either BC or BrC (Forrister et al., 2015; Yu et al., 2019), this selection of refractive indices provides reasonable upper and lower limits, covering all potential values, within this simulation.

λ (nm)	Sulfuric Acid	BC	BrC
385	1.448 + 0i	1.75 + 0.50i	1.55 + 1.0E-2i
450	1.434 + 0i	1.75 + 0.50i	1.55 + 4.4E-3i
520	1.431 + 0i	1.75 + 0.50i	1.55 + 2.6E-3i
600	1.430 + 6.38E-9i	1.75 + 0.50i	1.55 + 2.0E-3i
675	1.429 + 1.70E-8i	1.75 + 0.50i	1.55 + 2.0E-3i
755	1.427 + 7.59E-8i	1.75 + 0.65i	1.55 + 2.0E-3i
870	1.425 + 1.91E-7i	1.75 + 0.65i	1.55 + 2.0E-3i
1020	1.421 + 1.51E-6i	1.75 + 0.75i	1.55 + 2.0E-3i
1550	1.403 + 1.42E-4i	1.75 + 0.90i	1.55 + 2.0E-3i

Table 1. Complex refractive indices for smoke and sulfuric acid used in the Mie simulations. The smoke refractive index values were based on data collected by Bergstrom et al. (2002) for BC and Sumlin et al. (2018) for BrC. Sulfuric acid refractive index values are from Palmer and Williams (1975).

The simulation consisted of two parts: 1. assume a lognormal distribution with constant mode radius (200 nm) and constant distribution width (1.5) to visualize the expected extinction spectrum (panel (a) of Fig. 3); 2. assume a lognormal distribution with constant distribution width (1.5) and variable mode radius (40–500 nm) to visualize how the slopes changed as a function of particle size (panel (b) of Fig. 3). This was carried out for particles composed of sulfuric acid as well as varying mixtures of BC and BrC using the refractive indices in Table 1.

230   The results of this simulation are presented in Fig. 3 wherein it is observed that the ~~two species~~ smoke and sulfuric acid have different spectral behavior for extinction coefficients (panel a) and that the slopes were consistently different for small particle sizes~~,~~. especially when BC contributed to the smoke fraction (panel b). The vertical dashed line in Fig. 3 represents the mode radius for background sulfuric acid particles (Deshler et al., 2003), and the shaded region represents the range of expected smoke particle sizes (Moore et al., 2021). Here, we observed that addition of a small amount of BC (10%) significantly changed

235   the slope from pure BrC at small particle sizes. The minimum slope for the 90% BrC curve, within the range of expected smoke radii, corresponded to a mode radius of ≈200 nm for pure sulfuric acid particles. Within the context of this simulation, in order for sulfuric acid particles to be misidentified as smoke (here, 90% BrC and 10% BC), the sulfuric acid particles would have to have a mode radius of at least 200 nm. Therefore, while the sulfuric acid and pure BrC slope lines fall near to one another, addition of a small amount of BC reduces the ambiguity between the sulfuric acid and smoke curves.
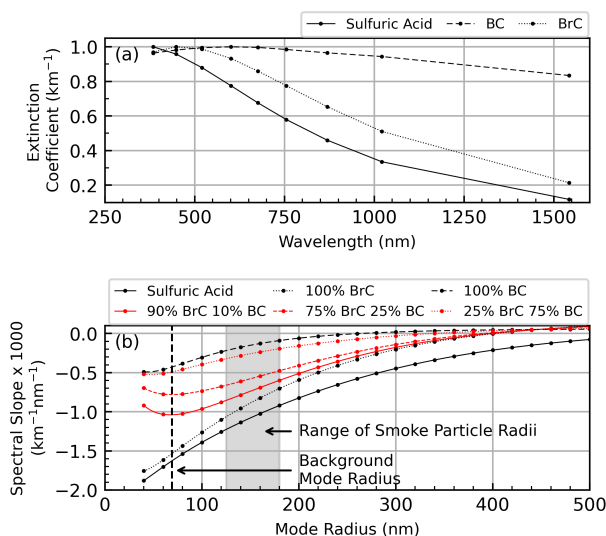
Figure 3. Spectra of extinction coefficients (normalized to 1) as a function of wavelength using a fixed mode radius of 200 nm and distribution width of 1.5 (panel a); spectral slope as a function of mode radius using a constant distribution width of 1.5 (panel b; see §5 for details on slope calculation) from the Mie theory simulation. Normalization in panel (a) was carried out by dividing each curve by its maximum value. The vertical dashed line in panel (b) indicates the background mode radius at 20 km, per Deshler et al. (2003). The gray-shaded region in panel (b) indicates a range of smoke particle radii (Moore et al., 2021).

240   We emphasize that this model is very simple, contains multiple assumptions, and presents a ~~general relationshipthat is in no way intended to be representative of actual conditions. Certainly, changing the smoke refractive indices from BC~~ generalized relationship. Further, smoke is composed of a highly variable mixture of BC and BrC that is dependent on burn conditions. Previous work has demonstrated the highly variable nature of the BrC refractive index (Alexander et al., 2008; Liu et al., 2015). While the real component of the BrC refractive index is spectrally flat, the values reported in the literature range from <1.4

245   to ~~BrC values significantly changed the extinction spectrum as well as the spectral slopes with the BrC slopes remaining~~

~~significantly different from sulfuric acid (≈2x smaller).~~ >1.85 (Kirchstetter et al., 2004; Müller et al., 2005; Alexander et al., 2008; Chakra[...]

making them comparable to BC. The imaginary component of the BrC refractive index is wavelength dependent (Kirchstetter et al., 2004; S[...]

and the range of reported values spans 1-3 orders of magnitude (e.g., see Fig. 4 of Liu et al. (2015) and references therein) with

the higher values approaching values comparable to BC. Therefore, the BrC refractive index values used within this simulation

250 are representative of the lower-end of the reported refractive indices. We recognize that the refractive indices for stratospheric BrC may be much closer to the BC values and we present Fig. 3 as indicative of a reasonable lower limit for the BrC extinction coefficients and spectral slope. Therefore, given this uncertainty in refractive indices, we explicitly state the caveat that Fig. 3 is neither intended to be representative of actual conditions nor is it presented as a predictive model. However, the model remains robust as a general guide for providing a testable hypothesis. While the details of the size distribution, refractive indices, and

255 number densities can modulate the differences in the slope, this has no impact on the subsequent analysis ~~.~~ because the data and assumptions used to generate Fig. 3 were not implemented in the upcoming analysis. Finally, we note that, as shown in panel (b) of Fig. 3, when particle sizes become large the slopes become less distinguishable because of the convergence of extinction coefficients at large particle sizes (as demonstrated by Thomason (1992) and Thomason et al. (2008) using extinction ratios). The consequence of this is that the current method is not applicable to large eruptions, such as the 1991 eruption of Mt.

260 Pinatubo, which result in the formation of large sulfuric acid particles. The ~~intent~~ sole intention of this simulation is ~~solely~~ to demonstrate that smoke ~~will~~ may have flatter spectra than sulfuric acid aerosol that is the product of small to moderate volcanic eruptions. ~~λ (nm) Sulfuric Acid BC BrC~~

~~385 1.448 + 0i 1.75 + 0.50i 1.55 + 1.0E-2i 450 1.434 + 0i 1.75 + 0.50i 1.55 + 4.4E-3i 520 1.431 + 0i 1.75 + 0.50i 1.55 + 2.6E-3i 600 1.430 + 6.38E-9i 1.75 + 0.50i 1.55 + 2.0E-2i 675 1.429 + 1.70E-8i 1.75 + 0.50i 1.55 + 2.0E-2i 755 1.427 +~~

265 ~~7.59E-8i 1.75 + 0.65i 1.55 + 2.0E-2i 870 1.425 + 1.91E-7i 1.75 + 0.65i 1.55 + 2.0E-2i 1020 1.421 + 1.51E-6i 1.75 + 0.75i 1.55 + 2.0E-2i 1550 1.403 + 1.42E-4i 1.75 + 0.90i 1.55 + 2.0E-2i~~

~~Complex refractive indices for smoke and sulfuric acid used in the Mie simulations. The smoke refractive index values were based on data collected by Bergstrom et al. (2002) for BC and Sumlin et al. (2018) for BrC. Sulfuric acid refractive index values are from Palmer and Williams (1975). Spectra of extinction coefficients (normalized to 1) as a function of wavelength~~

270 ~~(a) and spectral slope as a function of mode radius (b) from the Mie theory simulation.~~

What stood out most in this simulation was the stark contrast between the sulfuric acid and smoke aerosol types; i.e., the difference in how rapidly the extinction coefficients changed with wavelength. Indeed, the sulfuric acid values changed more rapidly than those for smoke, indicating that, when sulfuric acid aerosol is the predominant aerosol type, the overall slope of the extinction spectrum will be much larger (i.e., more negative) than when the atmosphere is laden with smoke. This distinction

275 provides a testable hypothesis to determine, preliminarily, the viability of separating smoke and sulfuric acid aerosol in real-world data. To this end, data collected during the four case-study events listed in Table 2 were used to see, broadly speaking, whether the different events showed consistent spectral differences. Data were selected for each event by truncating the data record to include profiles collected within $\pm 5°$ latitude of the event, and included data collected one month prior to, and three months after, the event (a four-month window) from 14–25 km. The extinction ratios (a proxy for spectral slope) for these four

280 events are presented as a function of k_{1020} in Fig. 4.

Event	Date	Latitude
Canadian wildfire	August 2017	52°N
Ambae eruption	April/July 2018	15°S
Raikoke mixed	June 2019	48°N
Ulawun eruption	June/August 2019	5°S
Australia wildfire	January 2020	35°S

Table 2. Listing of major events used in the current study. The Raikoke event is labeled as a mixed type because of the impact of coincident wildfires in Siberia and western Canada. All events used data collected between 14 and 25 km.
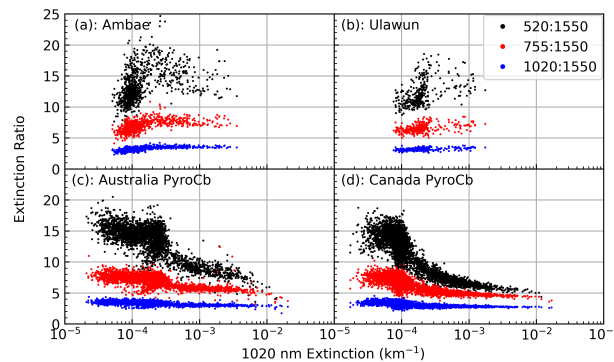
Figure 4. Extinction ratio plots, as a function of k_{1020}, for 3 ratios in the 4 case study events. All ratios were referenced to the 1550 nm channel and the data were limited to altitudes between 14 and 25 km.

Similar to the theoretical work (Fig. 3), the two volcanic events in the SAGE data (Fig. 4, panels a and b) showed very different behavior from the wildfire events (panels c and d). On one hand, as k_{1020} increased for the volcanic events the extinction ratio increased slightly, though it remained mostly unchanged, suggesting that both the composition and mean size of the optically important aerosol has remained unchanged from background (following Thomason et al. (2021)). On the other hand, the extinction ratios for the wildfire events had distinctly different behavior, quickly merging to smaller values (<10) as the extinction coefficient increased. This figure demonstrates that the measured extinction ratios behave as expected from the model and that, at least preliminarily, the two event types can be distinguished.

At this point we must reiterate the caveat that this holds true only for small or moderate eruptions and would not be applicable to larger eruptions such as the 1991 eruption of Mt. Pinatubo. Eruptions that inject large amounts of ash and SO$_2$ into the stratosphere, like Pinatubo, have been observed to rapidly produce extinction ratios indistinguishable from water clouds and presumably smoke. This process involves the conversion of SO$_2$ to gaseous sulfuric acid (e-folding time of ≈30 days) which then either deposits on to existing aerosol or nucleates to form many small particles that coagulate to form optically large aerosol. Indeed, the first SAGE II observations of the main Pinatubo plume (when transmission was not saturated) showed a

525 to 1020 nm extinction coefficient ratio of essentially 1 (Thomason, 1992). However, within the framework of the current study we only consider relatively smaller eruptions that inject much less SO_2 into the stratosphere, with Raikoke (VEI-4) being the largest.

Up to now we have only considered the raw extinction spectrum (e.g., Fig. 3 (a)) and a simple combination of extinction coefficients expressed as the extinction ratio (Fig. 4). This was useful for comparing measurements to theory and for providing rudimentary visualizations, though it requires the analysis to be done on a channel-by-channel or extinction ratio-by-extinction ratio basis (hence the three colors in Fig. 4). Indeed, using a single extinction ratio (e.g., $k_{520} : k_{1020}$) yielded results that were similar to the spectral-slope approach. However, all of the information in these ~~four~~ three ratios can be efficiently combined into a single number within the spectral slope, thereby eliminating the channel-by-channel approach, streamlining the analysis, mitigating the potential for noise in a single channel to influence the outcome, as well as mitigating the impact of the low bias in the k_{520} channel. Therefore, given the consistent behavior between the model and the measured extinction ratios we ~~hypothesize~~ hypothesized that small-to-moderate volcanic eruptions that inject material into the stratosphere can be distinguished from wildfire events in the SAGE record by looking at the spectral slope. ~~Event Date Altitude (km) Latitude~~

~~Canadian wildfire August 2017 14-25 52N Ambae eruption April/July 2018 14-25 15S Raikoke mixed June 2019 14-25 48N Ulawun eruption June/August 2019 14-25 5S Australia wildfire January 2020 14-25 35S~~

~~Listing of major events used in the current study. The Raikoke event is labeled as a mixed type because of the impact of coincident wildfires in Siberia and western Canada. The altitude column refers to the altitude range used in creating Fig. 4. Extinction ratio plots, using 3 ratios, for the four case study events. All ratios were referenced to the 1550 nm channel.~~

5 Detection and classification method

To test the aforementioned hypothesis, we evaluated the change in spectral slope as a function of k_{1020} for 4 case-study events (2 pyroCb, 2 volcanic; see §6 for details). To do this, the spectral slope was calculated via linear regression where channel wavelength (nm) acted as the independent variable and $\log_{10}(\boldsymbol{k})$ was the dependent variable. The 385 channel was excluded from this analysis because of its rapid attenuation at relatively high altitudes ($\approx$18 km). The 600 and 675 nm channels were excluded from the linear regression due to the impact ozone has on these aerosol channels. Further, to reduce the influence of potentially spurious measurements, a conservative cutoff was applied by excluding all extinction coefficients that had relative error >20% and we only used extinction spectra that had valid values in the 6 remaining channels (i.e., 450, 520, 755, 870, 1020, 1550 nm). These slopes were evaluated for each case study event and the results were then applied to the Raikoke event to distinguish between sulfuric acid aerosol and smoke within this single event (see §7).

Not all profiles collected after a volcanic or wildfire event were impacted by that event. Therefore, a method for discriminating between background and perturbed conditions was developed. The use of median $(\tilde{X})$ and median absolute deviation (MAD) has become a popular, statistically robust, alternative to using mean and standard deviation for the elimination of outliers and their impact on an analysis (Leys et al., 2013). If the sample population is normally distributed, then MAD $\cdot$ 1.4826 is equivalent to 1 standard deviation (~~1-σ~~ 1σ). Therefore, we implemented a more rigorous definition of MAD (labeled MAD*,

$\approx 2\cdot\sigma \cong 2\sigma$) as defined in Eq. (3) where $b = 2 \cdot 1.4826$ and $\boldsymbol{x}$ is an array of the dataset under investigation.

$$\text{MAD}^* = b \cdot \text{median}(|\boldsymbol{x} - \tilde{X}|) \tag{3}$$

Herein, the median and MAD* of the spectral slopes ($\tilde{X}_m$, MAD$^*_m$) and k_{1020} ($\tilde{X}_k$, MAD$^*_k$) collected during background periods were calculated for each event, as a function of altitude, using data collected within 5° of the each event's latitude. Initially, the background statistics were calculated using only the month prior to each event, but that provided insufficient sampling for the Ambae and Ulawun events due to SAGE's observation schedule (see, for example, Fig. 1 of Knepp et al. (2020)). Therefore, the background time period for the Ambae and Ulawun events was expanded to include 9 months prior to the eruption. The Ulawun eruption required an additional modification. Ambae and Ulawun are geographically close ($\approx$2000 km) and Ulawun erupted within a year of Ambae's last eruption. Therefore, the stratosphere was still recovering in the months prior to the Ulawun eruption, which biased the background statistics. Background statistics for Ulawun were calculated using profiles collected in Ulawun's latitude band ($\pm 5°$), but using data collected in the 9 months leading up to the Ambae eruption.

Spectra were assigned one of 3 classifications based on the following criteria (here, $\tilde{X}$ and MAD* refer to background conditions):

1. **Background:** When extinction was not enhanced. i.e.,

$$k_{1020} \leq \tilde{X}_k + \text{MAD}^*_k$$

2. **Sulfuric acid aerosol:** When extinction was enhanced, and the slope was less than (i.e., more negative) or equal to the background slope.

$$(k_{1020} > \tilde{X}_k + \text{MAD}^*_k) \text{ \& } (\text{slope} \leq \tilde{X}_m + \text{MAD}^*_m)$$

3. **Smoke:** When extinction was enhanced and the slope was flatter than background conditions.

$$(k_{1020} > \tilde{X}_k + \text{MAD}^*_k) \text{ \& } (\text{slope} > \tilde{X}_m + \text{MAD}^*_m)$$

A shortcoming of this classification scheme is that it uses hard cutoff values to separate the aerosol types while, in reality, particles near the smoke/sulfuric acid cutoff would likely be a mixture of the two and not strictly homogeneous. However, the utility of this method, as described, makes the identification of smoke highly conservative.

5.1 Layer identification with CALIOP

Ideally, this characterization scheme would be validated with in situ sampling of the various and disparate aerosol layers, which requires expansive sampling on a global (or at least a hemispherical) scale that is not feasible. However, the CALIOP lidar has polarization sensitivity at 532 nm ~~which~~ that can be used to make general composition estimates (e.g., sulfuric acid aerosol, smoke, dust, cloud, and volcanic ash). Smoke injected into the stratosphere due to pyroCb events can be discriminated from

sulfuric acid aerosol based on the level of depolarization in the return signal (Kim et al., 2018). The ratio of the perpendicular and parallel polarized components of the backscatter (depolarization ratio), provides information about the shape of the scattering particles. In general, the depolarization ratio of tropospheric smoke is quite low (<0.05). However, ~~the depolarization ratio of~~ smoke detected in the stratosphere from pyroCb events ~~have~~ has much higher depolarization ratio (0.1-0.2, per Christian et al. (2020)). This feature can be used to separate stratospheric smoke from the volcanic sulfate particles which are spherical and ~~thus do not depolarize.~~ have only low particulate depolarization ratio (< 0.1). Prata et al. (2017) found mean particulate depolarization ratios of 0.09 and 0.05 for the sulfates from Kasatochi and Sarychev volcanoes. In addition to depolarization ratio, the CALIOP data products contain a vertical feature mask (VFM) product that classifies the different types of detected layers as aerosol (tropospheric and stratospheric) and clouds (Vaughan et al., 2018). Both depolarization ratio and the VFM were used herein to corroborate the identification of sulfuric acid aerosol and smoke within the SAGE data.

5.2 Potential misclassifications in mixed events

In theory, the proposed classification method is straight forward and is expected to be reliable for events of a single type (i.e., either volcano or wildfire, but not necessarily mixed events). However, when both volcanic and wildfire events occur within the same time frame and latitude band the chance for mixing is high, leading to ambiguous determinations of composition. For example, the method presented in this manuscript only considers the integrated properties of the identified aerosol layers and cannot partition out the relative contribution of each aerosol type. Therefore, if smoke mixes with a sulfuric acid plume then we observe the total extinction of that layer and, based on the corresponding slope of the extinction coefficient spectrum, that layer is classified as either smoke or sulfuric acid; this is a false dichotomy.

Figure 5 demonstrates how the spectral slope can change as a function of smoke fraction, relative to pure sulfuric acid aerosol. This simulation was carried out for 2 sulfuric acid distributions to represent 2 scenarios: 1. smoke was injected into the background stratosphere, in the absence of recent volcanic activity (mode radius of sulfuric acid aerosol was set to 70 nm); 2. smoke was injected into the stratosphere when sulfuric acid particle sizes were larger because of recent volcanic activity (mode radius of sulfuric acid aerosol was set to 150 nm). In both of these scenarios the smoke particle mode radius was fixed at 200 nm, and all distributions had widths of 1.5. This was carried out for 5 different smoke compositions that had varying degrees of BC content, similar to Fig. 3, thereby showing how the smoke composition may influence the magnitude of the relative change in slope with BrC having the smallest impact and BC having the largest, in agreement with Fig. 3. For example, according to Fig. 5, when 1% of the particles are smoke (99% are sulfuric acid particles) that is injected into a previously-perturbed stratosphere (i.e., when the mode radius of sulfuric acid particles is 150 nm) then the overall spectral slope will be changed by ≈1.8–7% as compared to pure sulfuric acid.

While we recognize that there are multiple assumptions built into this model, much like Fig. 3, we consider this to be a general guide for establishing our working hypothesis as well as interpreting the results of this analysis. Therefore, what Figs. 3 & 5 demonstrate is that a relatively small fraction of BC-containing smoke can significantly change the spectral slope, making it flatter. This change in slope is larger when the sulfuric acid particle size is at background levels (i.e., ≈70 nm per

Deshler et al. (2003)), which may be sufficient to push these values into the smoke classification. Therefore, this figure will used in the upcoming analysis to better understand potential misclassifications within the wildfire and Raikoke events.
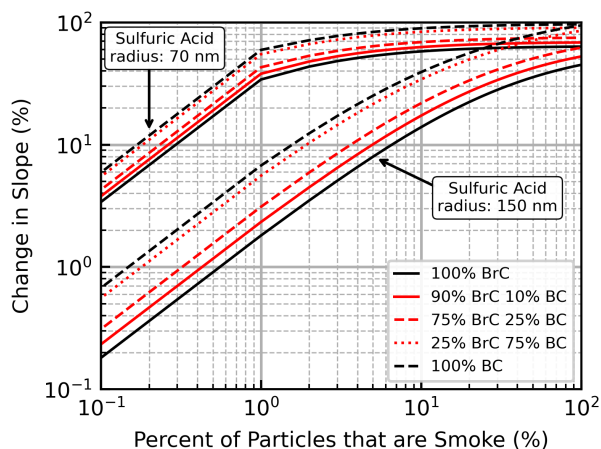
Figure 5. Change in spectral slope, relative to pure sulfuric acid aerosol, as a function of smoke fraction for 5 smoke compositions. Here, when 10% of the particles are smoke, the remaining 90% are sulfuric acid. The smoke particles had mode radius of 200 nm and distribution width of 1.5. The sulfuric acid distributions had a width of 1.5 and mode radii of 70 nm and 150 nm.

6 Application to case studies events

In this study we considered five events that had significant impact on the stratosphere as detailed in Table 2. Excluding Raikoke, these events were classified as either primarily volcanic or wildfire related, which provides four test cases for evaluating distinct behaviors for each event class. While the majority of the data collected for these events appears to come from a single source, we add the caveat that some events were close enough in time and geography to experience some carryover (e.g., the two Ulawun eruptions and the Australian pyroCb), which will be briefly discussed below.

To better appreciate the finer details of the profile data, and to demonstrate which parts of the atmosphere were most impacted by each event, the data were broken into 1 km bins. Statistics for labeling the different layer types in the 4 case-study events are presented in Table 3, which contains the total number of valid spectra collected at each altitude, the number of non-background spectra identified using the above cutoff criteria, and the fraction of enhanced spectra identified as either smoke or sulfuric acid aerosol.

6.1 Volcanic events

The classification scheme worked well for both volcanic case-study events as there were only 34 spectra mis-classified as smoke (out of >6400, ≈0.5%). It was observed that as extinction increased, the slopes tended to remain approximately consistent

		Altitude (km)											
		14	15	16	17	18	19	20	21	22	23	24	25
Ambae	Total Spectra	4	15	41	148	628	1391	1583	1586	1586	1586	1586	1586
	Enhanced Layers	0	3	17	51	249	479	479	339	189	48	8	0
	Sulfuric Acid	—	1.0	1.0	1.0	1.0	1.0	1.0	1.0	0.97	0.69	0.38	—
	Smoke	—	—	0	0	0	0	0	0	0.03	0.31	0.62	—
Ulawun	Total Spectra	0	1	2	29	205	755	889	892	892	892	892	892
	Enhanced Layers	0	1	2	18	154	627	867	883	855	704	395	34
	Sulfuric Acid	—	0	1.0	0.89	0.97	1.0	1.0	1.0	1.0	1.0	1.0	1.0
	Smoke	—	1.0	0	0.11	0.03	0	0	0	0	0	0	0
Canada	Total Spectra	2690	3194	3386	3546	3706	3794	3800	3800	3800	3800	3800	3800
	Enhanced Layers	2204	2669	2868	2957	2916	2808	2298	1689	1254	1267	1327	1217
	Sulfuric Acid	0.62	0.27	0.20	0.19	0.16	0.20	0.12	0.13	0.26	0.57	0.90	0.99
	Smoke	0.38	0.73	0.80	0.81	0.84	0.80	0.88	0.87	0.74	0.43	0.10	0.01
Australia	Total Spectra	3402	3789	3935	4029	4113	4135	4138	4138	4138	4138	4138	4138
	Enhanced Layers	2472	2885	3080	3204	3218	3142	2885	2710	2620	2441	2172	1865
	Sulfuric Acid	0.01	0.01	0	0.01	0.04	0.06	0.06	0.06	0.09	0.14	0.14	~~0.30~~ 0.40
	Smoke	0.99	1.0	1.0	0.99	0.96	0.94	0.94	0.94	0.91	0.86	0.86	0.60
Raikoke Primary	Total Spectra	1231	1483	1590	1631	1646	1652	1652	1652	1652	1652	1652	1652
	Enhanced Layers	969	1166	1236	1211	1078	753	329	344	389	387	261	123
	Sulfuric Acid	0.11	0.26	0.34	0.26	0.25	0.16	0.11	0.20	0.35	0.91	0.95	0.96
	Smoke	0.89	0.74	0.66	0.74	0.75	0.84	0.89	0.80	0.65	0.09	0.05	0.04
Raikoke Secondary	Total Spectra	10	32	69	185	458	812	896	896	896	896	896	896
	Enhanced Layers	10	28	54	127	319	484	471	380	60	108	218	125
	Sulfuric Acid	0	0.5	0.56	0.65	0.70	0.71	0.69	0.72	0.20	0.02	0.33	0.70
	Smoke	1.0	0.5	0.44	0.35	0.30	0.29	0.31	0.28	0.80	0.98	0.67	0.30

Table 3. Layer classification statistics from SAGE data. Total number of valid spectra, total number of identified layers as well as the fraction of spectra identified as smoke or sulfuric acid aerosol for each case-study event. For distinction between Raikoke Primary and Raikoke Secondary refer to §7.2.

with background slopes, or became slightly more negative as seen in Figs. 6 and 7. This moderate decrease in slope (i.e.,

shifting to more negative values) may be due to the formation of smaller particles immediately after the eruption. Indeed, Fig. 3 shows that smaller particles, regardless of composition, should lead to more negative slopes. Overall, there was little deviation from background conditions other than the enhanced extinction coefficient. This limited change in slope is reasonable because background stratospheric aerosol is composed of primarily sulfuric acid and the injection of SO_2 from moderately-sized volcanic events led to further formation of sulfuric acid aerosol. While this increased the overall extinction coefficient, its impact on the spectral slope was minimal due to the consistent composition and hence spectral properties under background and elevated loads.

We note that the Ulawun event had a small number of points that were classified as smoke with elevated k_{1020} between 17 and 18 km. While it is not unreasonable to have misclassifications, we note that these spectra were collected in January and February 2020, at the peak of the Australian wildfire, when smoke had transported over the Ulawun latitude range (Kloss et al., 2021). While we cannot definitively attribute these data points to smoke from the Australia pyroCb, the general pattern observed here (slope rapidly approached 0 with increasing extinction) is consistent with what was observed for the pyroCb events (*vide infra*) and we note this as interesting.

Though evidence for ash in the stratosphere, for these events, is tenuous, we cannot categorically exclude the possibility that ash was present in the stratosphere for at least part of each event's time period. However, if ash were present, it would result in more spectra being classified as smoke because, as discussed above, large particles tend to flatten the extinction spectra while enhancing k as was seen during Pinatubo. Indeed, this may be the cause of some of the smoke classifications in the Ulawun event mentioned above. However, particles of this size are not expected from these moderately-sized eruptions. Therefore, we conclude that ash and any other potentially large aerosol (sulfuric acid) ~~do~~ did not appreciably impact the optical measurements and that the majority of slopes presented in Figs. 6, 7 are reflective of small sulfuric acid aerosol only.

Figures 8 and 9 show examples of the CALIOP total attenuated backscatter at 532 nm (β_{532}; panel a), depolarization ratio (panel ~~a~~b), the CALIOP VFM (panel ~~b~~c), SAGE extinction profiles (panel ~~c~~d) as well as the SAGE spectral slope profile (panel ~~d~~e) for Ambae and Ulawun, respectively. The figure title provides the SAGE overpass date, latitude, longitude, and distance to the nearest CALIOP profile. The vertical arrow above panel (a) indicates the location of the SAGE overpass relative to the CALIOP curtain plot.

For both events, the peak in extinction corresponded well with a rapid decrease in spectral slope (i.e., became more negative) and a stratospheric aerosol layer identified in the CALIOP VFM between 17 and 19 km, and no significant depolarization, giving credence to the SAGE-based identification scheme for sulfuric acid aerosol.

6.2 Wildfire events

The wildfire events showed a mix of classifications, though the classification became uniformly smoke with increasing k_{1020}, as shown in Figs. 10 & 11. Further, as compared to background conditions, the slopes changed by up to 80%~~.~~, which corresponds to predominantly smoke particles that are composed of primarily BC (Fig. 5). The lowermost altitudes for the Australia events showed a nearly monolithic identification of smoke, as well as a distinct separation from background conditions, which makes
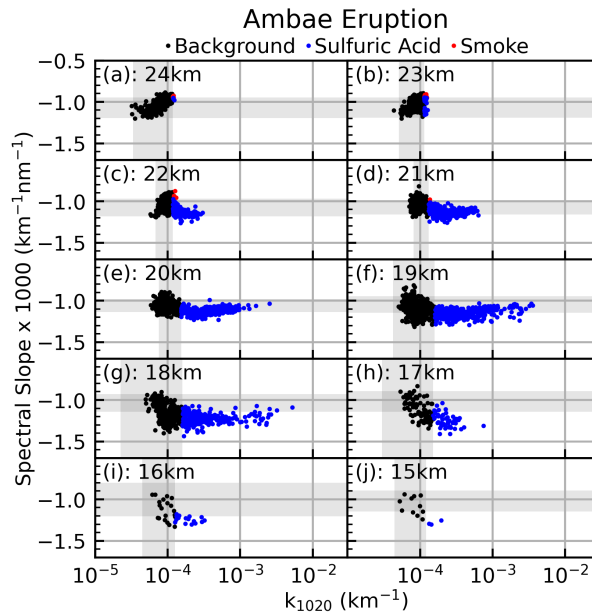
Figure 6. Spectral slope (x1000) as a function of k_{1020} and altitude for data collected over the Ambae eruption. The gray shaded regions indicate the width of MAD* as described in Eq. (3).

sense since the lowermost altitudes are the most impacted by these events. The Canadian wildfire likewise showed a nearly uniform identification of smoke at elevated k_{1020}.

440   While the volcanic events showed nearly uniform identification of sulfuric acid aerosol under elevated conditions, the wildfire events showed a significant portion of the spectra identified as sulfuric acid aerosol ($\approx$10,000 out of >58,000; $\approx$19%). Of these $\approx$10,000 sulfuric acid classifications, $\approx$48% of them were in the Canadian wildfire event ~~between 23 and 25 km~~within a narrow altitude range (23–25 km). The reason for the presence of elevated sulfuric acid aerosol within the wildfire events could be for two reasons. First, within the current identification scheme, it is possible for smoke to be ~~identified~~ misclassified as sul-

445 furic acid because of the combination of the SAGE viewing geometry and the optical thinness of parts of the smoke plume (i.e., depending on whether SAGE is sampling through the centroid of the plume or only the outer edge where the smoke fraction is low). It is reasonable that, when sampling optically thin smoke layers, the extinction will be elevated above background levels, but the slope may not deviate significantly. This can be achieved when the viewing geometry is such that ~~only optically thin portions~~ the path length through an optically thin portion of the smoke plume ~~are~~ is sampled, thereby raising the extinction

450 coefficients, but the ~~overall, integrated aerosol along the viewing path is not sufficiently different from background conditions to significantly change the spectral slope . This could~~ spectral slope remains effectively unchanged because of the paucity of smoke particles within this layer. This may lead to an ambiguous characterization of aerosol composition at extinctions that are outside background values, but still at the lower end of extinction values for that particular event as seen in Figs. 10 & 11. This scenario is the most likely and is ~~expected~~ not unexpected from a statistical viewpoint. Secondly, a less likely scenario is there
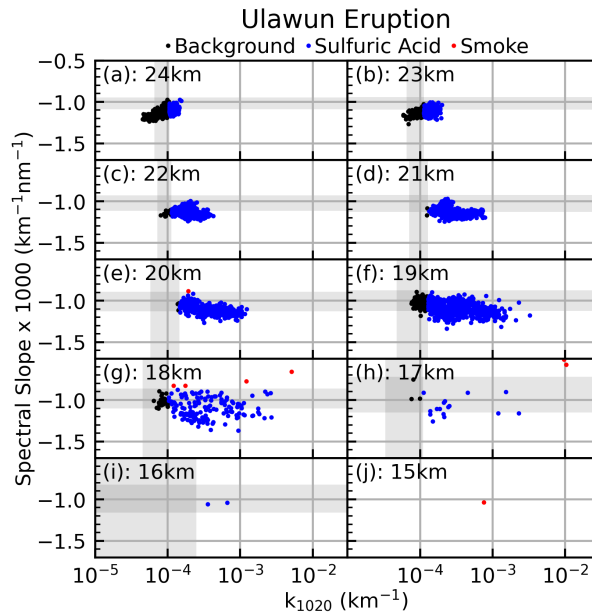
Figure 7. Same as Fig. 6, but for the Ulawun eruption.

455   may be elevated levels of sulfuric acid aerosol within the sampling volume due to transport from a nearby and recent volcanic

event. Indeed, this may be the case for some of the spectra classified as sulfuric acid in the Australian wildfire case study. In

contrast to the Canadian wildfire, the range of background extinction coefficients for the Australian fire spanned a wider range

and extended into higher extinction coefficients (e.g., >5E-4 at 16 km), indicating the apparent background conditions were

perturbed, potentially from the 2019 Ulawun eruptions (Kloss et al., 2021). If this is the case, then it reasonable for the sulfuric

460   acid particles to be larger than they would be under background conditions, and the potential impact this has on the change

in spectral slope can be seen in Fig. 5. Regardless of why spectra were classified as sulfuric acid, the performance of this

identification scheme remains encouraging as the majority (>81%) of non-background values were identified as smoke within

~~these~~ the enhanced layers as shown in Table 3. Further, the distribution of data for the wildfire events is markedly different

from the volcanic events, indicating that we are observing two distinctly different aerosol types.

465   Figures 12 and 13 show examples of the CALIOP and SAGE profile data collected over the two wildfire case-study events.

Here, CALIOP showed significant depolarization near 19 km (Canadian pyroCb) and 14 km (Australian pyroCb), which

corresponded well with a rapid increase in both aerosol extinction and spectral slope in the SAGE profile data. We note that in

Fig. 13 SAGE saw another layer at 19 km that was not manifest within the CALIOP ~~VFM or depolarization ratio profiles~~data.

This altitude is well within the SAGE instrument's operational altitude range and may be reflective of the relatively poor return

470   signal at this altitude for CALIOP and its narrow swath width. Alternatively, SAGE may have sampled a narrow smoke filament

that was not within the CALIOP sample volume.
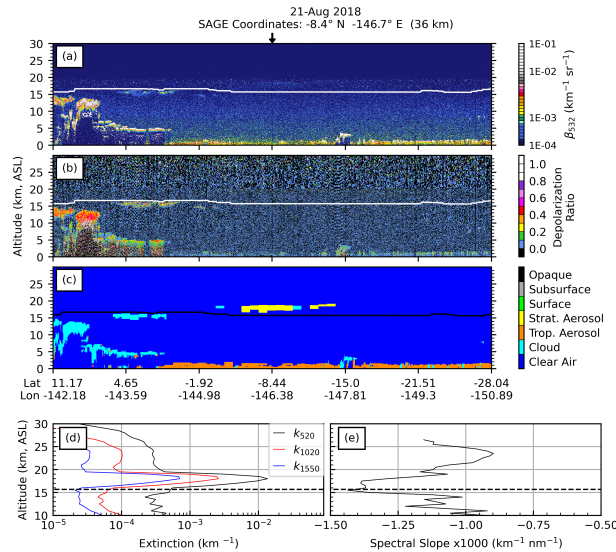
Figure 8. CALIOP and SAGE data collected during the Ambae eruption. The title indicates the SAGE profile date, SAGE overpass coordinates, and the distance between the SAGE profile and the nearest CALIOP profile. Panel (a) presents the CALIOP L1 total attenuated backscatter at 532 nm; Panel (b) presents the CALIOP L1 depolarization ratio; Panel (c) presents the CALIOP L2 VFM; Panel (d) presents the SAGE extinction coefficient profiles at 3 wavelengths; and Panel (e) presents the spectral slope profile of the SAGE extinction spectrum. The vertical arrow above panel (a) indicates the location of the SAGE profile along the CALIOP flight path. Solid horizontal lines (panels a~~and~~, b, and c) and dashed horizontal lines (panels d and e) indicate tropopause altitude. The CALIOP granule used to generate this image is CAL_LID_L1-Standard-V4-10.2018-08-21T11-04-30ZN.

Overall, the CALIOP data products provided good support for the SAGE-based classification of stratospheric aerosol composition for case studies that were unambiguously single-sourced and when the volcanic events were moderate in size. Therefore, this identification scheme will now be applied to a ~~much more heterogeneous~~ more complicated event: the 2019 Raikoke eruption.

7 Application to the Raikoke event

7.1 Smoke present in stratosphere prior to Raikoke

Though there were ~~two~~ multiple pyroCb events in the northern hemisphere during the summer of 2019 (e.g., Siberia and western Canada per ~~Kloss et al. (2021)~~ Bachmeier, Scott (2019), Johnson et al. (2021), Kloss et al. (2021), and Vaughan et al. (2021)), there were no wildfire events of similar magnitude as the 2017 Canadian wildfire or the 2020 Australian burn. However, Vaughan et al. (2021) ~~claimed they may have observed~~ reported observing stratospheric smoke prior to the Raikoke eruption, Kloss et al. (2021) suggested the ~~NH~~ northern hemisphere wildfires impacted the stratosphere, and ~~Bachmeier, Scott (2019)~~
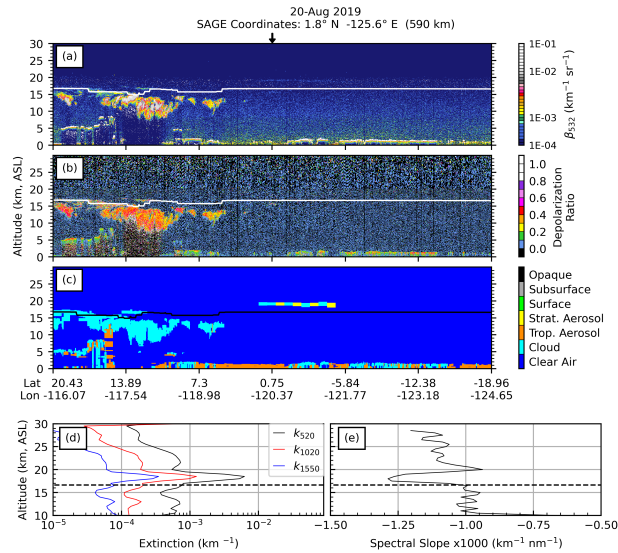
Figure 9. Same as Fig. 8, but for the Ulawun eruption. The CALIOP granule used to generate this image is CAL_LID_L1-Standard-V4-10.2019-08-21T09-34-46ZN.
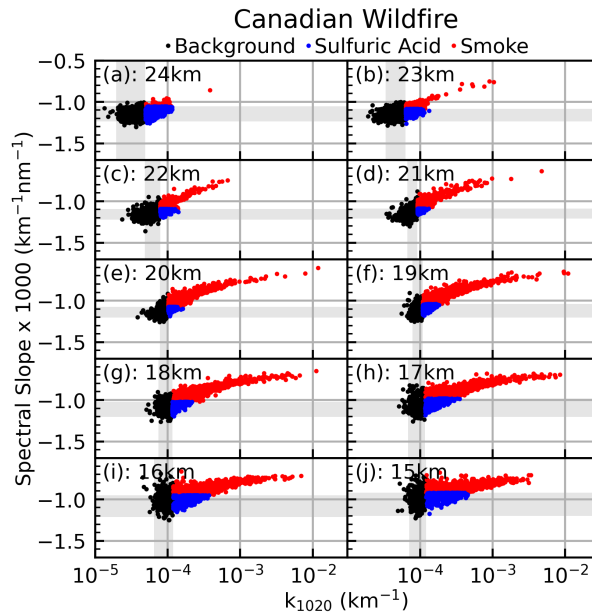
Figure 10. Same as Fig. 6, but for the Canadian wildfire.

classified the Siberian wildfire near Lake Bolon as a pyroCb. Similarly, smoke was identified in the lower stratosphere via
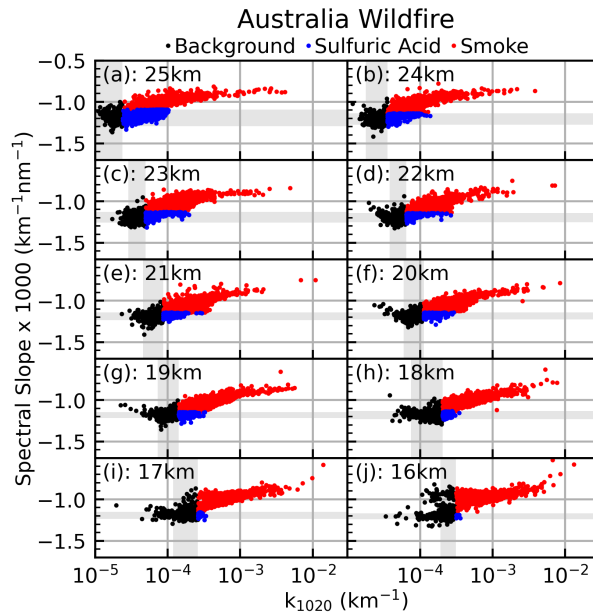
Figure 11. Same as Fig. 6, but for the Australian wildfire.
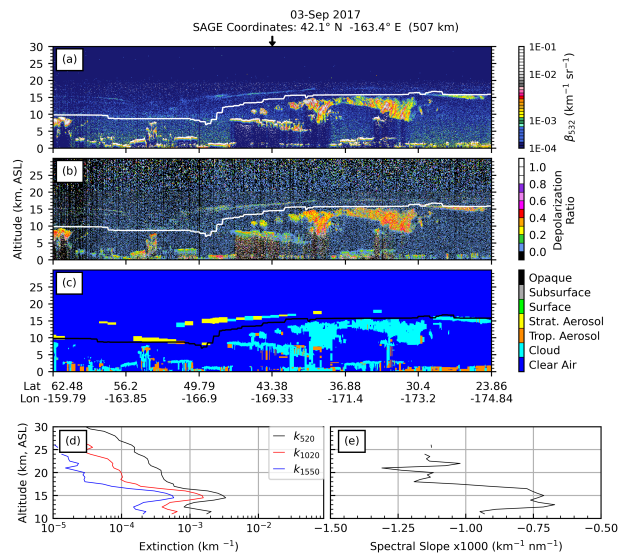
Figure 12. Same as Fig. 8, but for the Canadian pyroCb. The CALIOP granule used to generate this image is CAL_LID_L1-Standard-V4-10.2017-09-04T13-24-46ZN.

CALIOP, ground-based and shipborne lidar observations (Ansmann et al., 2021; Ohneiser et al., 2021). To further support the
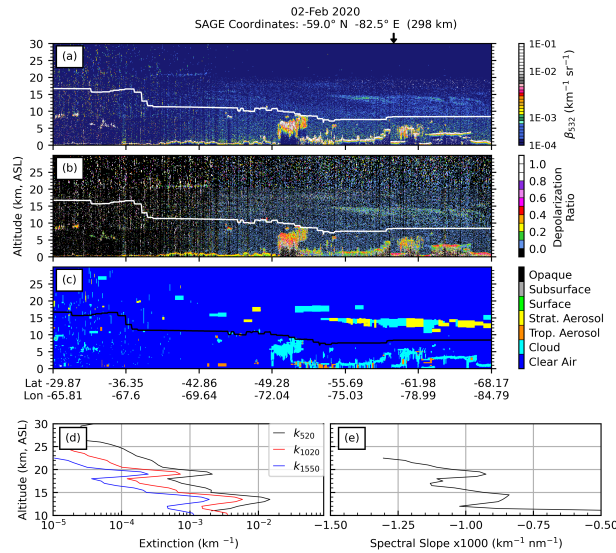
Figure 13. Same as Fig. 8, but for the Australia pyroCb. The CALIOP granule used to generate this image is CAL_LID_L1-Standard-V4-10.2020-02-02T05-24-58ZN.

485 fact that smoke was in the stratosphere prior to the Raikoke eruption we applied our method to identify an unambiguous smoke signal in the stratosphere ~~prior to, or immediately coincident with,~~ soon after the Raikoke eruption. To this end, we evaluated SAGE and CALIOP data collected to the west of Raikoke (i.e., upwind, see Fig. 14). Unfortunately, SAGE did not begin sampling this latitude band until after the eruption, therefore we limited our analysis to the first two weeks after the eruption and to a region far enough west of Raikoke to not have been impacted by the volcanic ejecta (Kloss et al., 2021).

~~Both SAGE and CALIOP collected profiles within this region and indicated the presence of smoke at ≈13 km as seen in~~
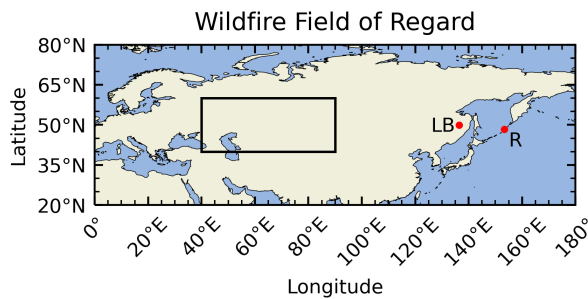
Figure 14. Field of regard for sampling air that has not been impacted by the Raikoke event, but may have been impacted by coincident northern hemisphere wildfires. LB and R indicate location of the Lake Bolon, Siberia fire and Raikoke, respectively.

490

The CALIOP backscatter profile (Fig. 15. ~~These profiles were collected within 8 days of the eruption, while the plume still resided over the North Pacific ocean (Kloss et al., 2021; Vaughan et al., 2021). This enhancement was most noticeable in the CALIOP~~, panel (a)) showed enhanced backscatter from 10–15 km (42°N and 55°N) that had significant depolarization (Fig. 15, panel (b)), indicative of stratospheric smoke. Based on this enhanced backscatter, we expected enhanced extinction in the

495 SAGE data as well ~~as the spectral slope profile~~. Indeed, ~~the spectral slope shows a sharp gradient at this altitude, before returning to background conditions between 15 and 20 km (compare to background conditions during the 2017 Canadian pyroCb event, Fig. 12), while the CALIOP depolarization ratio and VFM showed a distinct layer~~ enhanced extinction was observed at ≈11 km and 19 km, with a minor enhancement at 15.5 km (Fig. 15, panel (d)). The spectral slope (Fig. 15, panel (e)) indicated the presence of smoke from ≈10–15 km (i.e., where slope >-0.001 km^{-1} nm^{-1}), but did not indicate smoke for the layers at 15.5

500 km or 19 km, in agreement with the CALIOP data. Overall, both SAGE and CALIOP indicated smoke was present between 10 and 15 km. ~~Therefore, while the~~, though the backscatter and extinction profiles showed different features (e.g., SAGE saw a layer at 20 km while CALIOP did not). This is not unexpected because of the distance between the 2 measurement locations (482 km). Regardless of these minor differences, both instruments clearly showed enhanced smoke above the tropopause over a region that was yet to be impacted by the Raikoke eruption (i.e., at this time the Raikoke plume was still located to the east of

505 the North Pacific Ocean and Canada as shown in Fig. 1, Kloss et al. (2021), and Vaughan et al. (2021)). While the SAGE sampling schedule did not allow us to evaluate profiles collected within this region prior to this time, this smoke layer was persistent over this region, in both the SAGE and CALIOP records, throughout the first ≈2 weeks after the eruption ~~and we concur with previous authors that smoke was present in the stratosphere~~ (data not shown). This is in agreement with previous studies that reported observing stratospheric smoke between 8 and 13 km between 50°N and 85°N during this time period ~~and was visible in~~

510 ~~both the SAGE and CALIOP profiles~~ (Ansmann et al., 2021; Johnson et al., 2021; Ohneiser et al., 2021; Osborne et al., 2021; Vaughan et a .

7.2 Raikoke ~~main~~ primary peak

As stated in the introduction, Raikoke erupted on 22-June 2019 and injected SO_2 and ash directly into the stratosphere, at around 15 km altitude, with SO_2 detected shortly thereafter at 19 km (Hedelt et al., 2019), and was observed by SAGE ap-

515 proximately one week later (Fig. 1). Immediately after the eruption, the ~~main~~ primary Raikoke plume broke into two distinct plumes. One plume moved southward and appeared to be primarily ash as determined by Kloss et al. (2021) and Vaughan et al. (2021). The ash in this plume settled out within a week of the eruption (Kloss et al., 2021). The second plume, however, moved to the north and east and was composed primarily of SO_2 (Kloss et al., 2021), ~~(which was in the process of being converted into sulfuric acid) before getting temporarily trapped within the Aleutian low (Kloss et al., 2021). This~~. The bulk of this SO_2

520 plume remained between Kamchatka and Alaska for 2-3 weeks (de Leeuw et al., 2020; Vaughan et al., 2021) before moving eastward over the United States, the UK, and Europe. Therefore, similar to the case-study events, data collected near Raikoke's latitude (48°N, ±5°) and within 7 months after the eruption were used in this analysis. Because of the broad time range and the lack of longitudinal limitations there were a non-negligible number of spectra that fell into the background classification, similar to the case-study events.
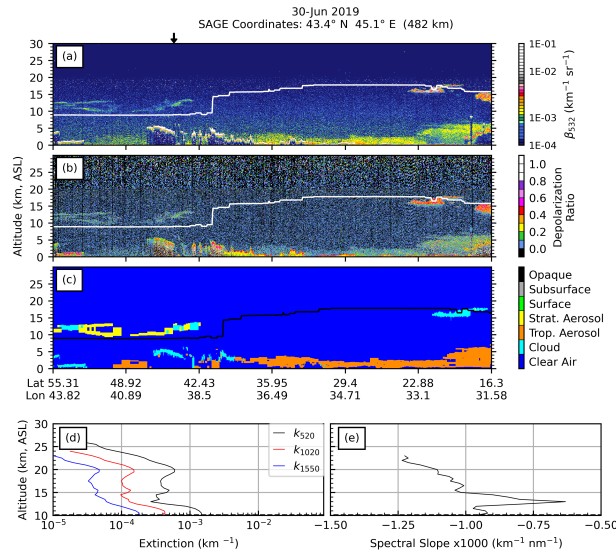
Figure 15. ~~Field of regard for sampling~~ Smoke identified within an air mass that has ~~not been~~ yet to be impacted by the Raikoke ~~event~~eruption, but ~~may have been impacted by coincident NH wildfires. LB and R indicate location~~ was sampled within 8 days of the ~~Lake Bolon, Siberia fire and~~ Raikoke ~~, respectively~~eruption. The CALIOP granule used to generate this image is CAL_LID_L1-Standard-V4-10.2019-06-29T23-42-21ZN.

~~Smoke identified within an air mass that has yet to be impacted by the Raikoke eruption, but was sampled within 8 days of the Raikoke eruption.~~

525 Based on the results presented in the previous section, we anticipated that the spectral slopes of the SAGE data collected over the Raikoke event would behave similar to those for Ambae and Ulawun. However, as shown in Fig. 16 and Table 3 the Raikoke data presented what appears to be a mixture of sulfuric acid aerosol and smoke, with the predominant ~~composition~~ classification being smoke (only 10-30% of spectra were identified as sulfuric acid aerosol). Indeed, the majority of lower-altitude spectra were identified as smoke, while the balance ~~seemed to shift~~shifted to sulfuric acid at the highest altitude (23

530 km). While we anticipated observing smoke within the profiles we did not expect the majority of the spectra to be identified as such. ~~Overall,~~ Based on this general classification scheme the Raikoke data ~~look~~looked more like a wildfire event than the other volcanic events in this study. Given the magnitude of this eruption, the spectra identified as smoke here may be the product of ~~both ash and~~ash and/or large particle formation~~, both of which have short lifetimes in the stratosphere~~. The potential for misclassifying these layers is discussed in §7.4.

535 **7.3 Interpretation of the secondary Raikoke plume**

As shown in Fig. 2, a secondary layer of elevated aerosol broke off from the ~~main~~primary Raikoke plume as it moved southward and continued to loft to higher altitudes. ~~The~~ We hypothesized that the composition of this secondary plume ~~was speculated to~~would contain smoke from ~~NH~~northern hemisphere wildfires, which would cause it to absorb incoming solar radiation,
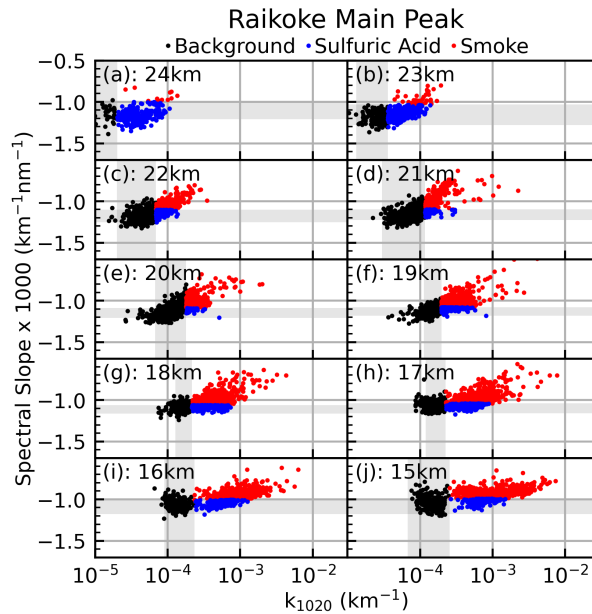
Figure 16. Same as Fig. 8, but for the Raikoke eruption.

warm the surrounding air, and diabatically loft. This layer continued to circle the globe before it reached a maximum altitude

540   between 23 and 25 km between 10 and 25°N (Chouza et al., 2020). Extinction spectra collected by SAGE between 10°N and 30°N (within 7 months of the eruption) were evaluated to determine the composition of this secondary plume. The results of the altitude-based classification are presented in Fig. 17 as well as the statistics in Table 3.

     It is important to recall that the atmosphere had a mixture of aerosol compositions within the Raikoke time period~~and~~, that a relatively small contribution of smoke can significantly influence the spectral slope~~as well as k~~, and the degree of this influence

545   is dependent on refractive index~~.~~, smoke particle size, and pre-event sulfuric acid particle size as shown in Fig. 5. Needless to say, the overall situation is complex with many competing factors. Therefore, the interpretation of Fig. 17 must be done with caution and we have tried, prior to this point, to lay the foundation for this interpretation. In §~~7.2 we explained how spectra classified as sulfuric acid may have a smoke influence~~6.2 we discussed how smoke spectra may be influenced by sulfuric acid. Further, we discussed the false dichotomy of labeling particles as *either* sulfuric acid *or* smoke in §5.2. This was done with

550   a mixed event, such as the Raikoke time period, in mind. Applying this reasoning to the secondary peak allows us to provide a reasonable interpretation of Fig. 17, and we ask the reader to understand that we are not suggesting the data in this case be interpreted as *either* sulfuric acid aerosol *or* smoke; rather it is plausible that there are contributions from both throughout the profiles as well as the possibility of ash.

     We observed distinctly different patterns between the two case-study event types (i.e., slightly decreasing or near-constant

555   slope with increasing extinction for volcanic events (Figs. 6, 7) and flattening of slope with increasing extinction for wildfire events (Figs. 10, 11)). Both of these general patterns were observed in profiles used in creating Fig. 17, sometimes at the
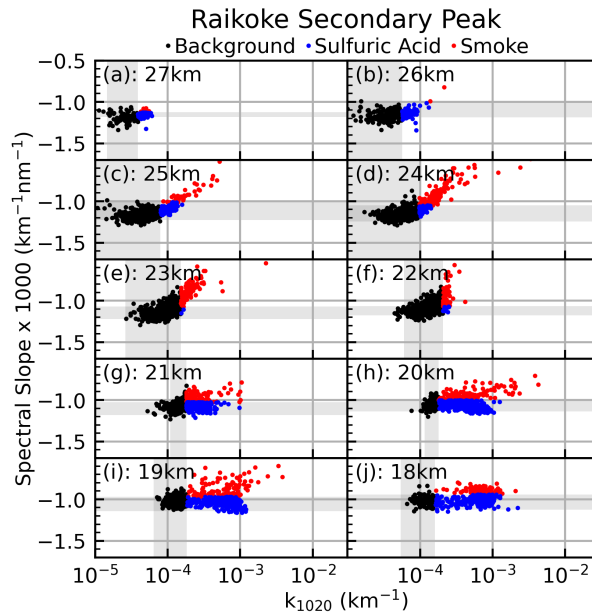
Figure 17. Same as Fig. 6, but for the elevated layer that broke off the ~~main~~ primary Raikoke plume and continued to ascend as it moved southward.

same altitude. For example, the data at ~~18 and~~ 19 and 20 km showed both patterns, which led to a bifurcation in slope at higher extinction coefficients. We interpret this as a mixture of smoke and sulfuric acid aerosol at these altitudes, though not necessarily at the same longitude (i.e., the smoke and sulfuric acid were not necessarily part of the same airmass). That said, what stood out in Fig. 17 was the dominance of sulfuric acid aerosol at the lowermost altitudes ($\leq$21 km) and the stark transition to a predominantly smoke classification at higher altitudes (e.g., >98% at 23 km)~~where the secondary plume was observed~~. This transition was most notable between 21 and 25 km where the slope rapidly changed (Fig. 17, panels c-g). While ~~smoke was identified~~ particles were classified as smoke throughout the profile, this partitioning is representative of the behavior that may be expected from single-source events: the absorbing species (smoke) rose to higher altitudes while the non-absorbing species (sulfuric acid) was carried along the same altitude. ~~Further, the presence of smoke throughout the profile demonstrates that the smokey air mass did not traverse through the atmosphere in an isolated manner. Rather, this air mass interacted with the surrounding atmosphere by shedding smoke and likely acquiring sulfuric acid aerosol as it ascended.~~

Unfortunately comparison with CALIOP was not possible for the secondary plume. Due to the sparseness of SAGE coverage in the tropics an observation that was collocated with CALIOP was not found. ~~However,~~ While Chouza et al. (2020) demonstrated that elevated layers in this latitude band were observed from ~~Mauna Loa and CALIOP.~~ both the Mauna Loa ground-based lidar and CALIOP, the CALIOP depolarization ratio was too low to indicate smoke. The challenge in using the CALIOP depolarization ratio at these altitudes is the limited return signal. However, as will be shown below, there is the possibility that the smoke classifications may be incorrect.

7.4 Potential misclassification of Raikoke's sulfuric acid layers

Up to now the data collected during the Raikoke time period has been evaluated within the context of the single-source case study events. This was done with the perspective that the Raikoke eruption, which was significantly larger than the Ambae and Ulawun eruptions, would yield sulfuric acid particles of comparable size as Ambae and Ulawun. However, if we look at this event from another perspective (i.e., as a much larger eruption, it may have created larger sulfuric acid particles than Ambae and Ulawun), then there may be an alternative interpretation of the smoke classifications within the Raikoke data.

Another opportunity for identifying air masses that have been impacted by biomass burning events is to look for enhanced biomass-burning chemical tracers such as carbon monoxide (CO), and hydrogen cyanide (HCN), both of which are products within the ACE-FTS data (Boone et al., 2020). If an enhanced layer is identified within a profile, then individual ACE-FTS spectra can be analyzed to look for smoke-specific signatures (e.g., the carbonyl (C=O), hydroxyl (O−H), and C−H stretch features near $1{,}740$ cm^{-1}, $3{,}250$ cm^{-1}, and $1{,}740$ cm^{-1}, respectively; per Boone et al. (2020)). Using these criteria, we identified several profiles within the ACE-FTS record that showed enhanced biomass-burning tracers, a subset of which are presented in Fig. 18. Figure 18 shows ACE-FTS profiles of CO, HCN, and SO$_2$ that were collected within 2 months of the eruption between 24.5°N and 51.9°N. The climatological profiles were created by computing the average and standard deviation of the ACE-FTS products collected within the specified latitude ($\pm 2.5°$) and within the current season (i.e., July, August, September) using the entire ACE-FTS record. The open circles in Fig. 18 indicate the highest altitude at which smoke was identified using the carbonyl-stretch method as provided by the ACE-FTS team (C. Boone, personal communication, 2022). Finally, the SO$_2$ profiles were included to observe when the atmosphere was impacted by both wildfire and volcanic activity.

While Fig. 18 supports our finding that smoke was in the stratosphere during this time period and within the latitude range of our study, it does not provide confirmation for all of our smoke classifications. Indeed, we were unable to identify smoke or ash in the ACE-FTS data that were higher than ≈ 20 km, while the SAGE-based classification method identified more than 2,000 enhanced spectra above 20 km. One shortcoming of the ACE-FTS identification method is it is not automated and requires visual inspection of profiles for enhanced biomass-burning tracers followed by visual inspection for spectral residuals as described in Boone et al. (2020). Therefore, we recognize the possibility that additional smoke layers may be detected in the ACE-FTS data at altitudes higher than 20 km. While this is one possibility, there was one set of SAGE and ACE-FTS profiles (Fig. 19) there were exceptionally close in both space (difference of 32 km) and time (difference of 2 minutes) that allows for a direct comparison. Here, the SAGE classification algorithm indicated smoke from 12–19 km, while the ACE-FTS profiles showed no indication of biomass-burning tracers (only CO shown in Fig. 19). Further, individual ACE-FTS spectra were analyzed to determine if the carbonyl stretch feature was present, but it was not observed within this altitude range (C. Boone, personal communication, 2022). This is indicative of misclassification in the SAGE-based classification scheme.

The ACE-FTS team provided particle size estimates within this altitude range (assuming a sulfuric acid composition). The estimated radii spanned a relatively narrow range from 197 nm (15 km) to 230 nm (11 km). The SAGE data can likewise be used to infer particle sizes by comparing the slopes in Fig. 19 to the model presented in panel (b) of Fig. 3. This yielded particle
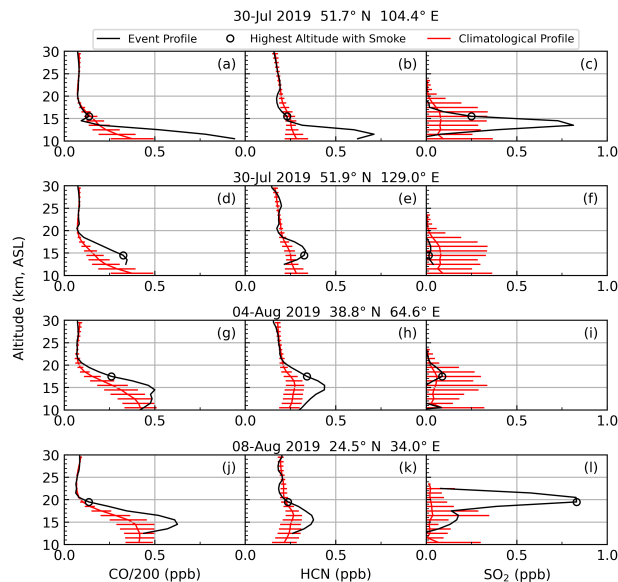
Figure 18. ACE-FTS profiles of CO (panels a, d, g, j), HCN (panels b, e, h, k), and SO_2 (panels c, f, i, l) collected within 2 months of the Raikoke eruption. The climatological profiles present the mean ± 1 standard deviation for data collected within the specified latitude ($\pm 2.5°$) for July/August/September over the lifetime of the ACE-FTS instrument. The open circles indicate the highest altitude at which the carbonyl stretch was identified (C. Boone, personal communication, 2022).

sizes of 160 nm (15 km) and 180 nm (12 km) with a maximum of 250 nm at 16 km. A third size estimate was performed using the method of Wrana et al. (2021) wherein the particle sizes were estimated to be consistently below 135 nm up to 20.5 km

610 and increased to 220 nm at 21.5 km (F. Wrana, personal communication, data not shown); significantly smaller than both the slope and ACE-FTS estimates. We recognize the challenges and limitations of such size inferences, so we do not present this information as definitive. Rather, we present this information to demonstrate the general disagreement between size distribution inference methods and note that further work is required for harmonizing the various inference techniques. We also note that this may lead to disparate conclusions being drawn regarding particle composition. On the one hand, the ACE-FTS estimates

615 do not require BrC or BC to be present in order to yield the observed slopes (compare slopes in panel (a) of Fig. 19 with the theoretical slopes near 200 nm in panel (b) of Fig. 3). On the other hand, the size estimates from the Wrana et al. (2021) method do require BrC or BC to be present to yield the observed slopes (compare slopes in panel (a) of Fig. 19 with the theoretical slopes near 130 nm in panel (b) of Fig. 3). As stated above, the ACE-FTS spectra showed no sign of smoke residuals. Therefore, we can reasonably rule out the presence of smoke within this profile. However, if we did not have the

620 benefit of a coincident ACE-FTS observation, which is the case for the majority of SAGE occultations, then the interpretation of the SAGE classifications, based solely on spectral slope and particle size estimates, would be more challenging. Certainly this highlights the need for ongoing work to better understand the applicability and veracity of these particle size distribution
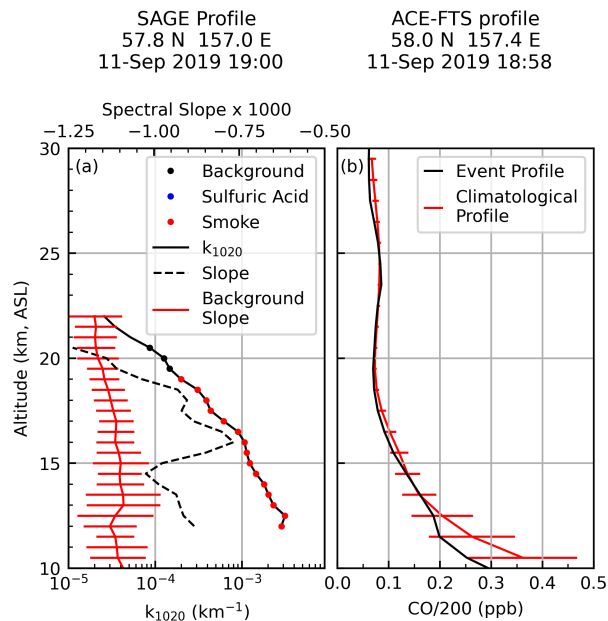
Figure 19. SAGE and ACE-FTS profiles collected in close proximity (both temporally and geographically). Colored dots in panel (a) indicated the SAGE-based composition classification. Panel (a) also shows the calculated spectral slope for this profile as well as the background slope values ($\tilde{X}_m \pm \mathrm{MAD}_m^*$). Panel (b) presents the ACE-FTS CO profile.

inference techniques as well as ongoing analysis of the Raikoke event to better understand the composition of stratospheric aerosol in the months subsequent to the eruption.

625 The question now at hand is: if the SAGE-based smoke classifications in the Raikoke event are in fact misclassifications, then why? We see two possibilities. First, the most immediate explanation would be that there were enough sulfuric acid particles to push k_{1020} out of the background classification and these particles were large enough to push the slope into the smoke classification. As seen in panel (b) of Fig. 3 and as discussed above, when sulfuric acid particles are large, the corresponding spectral slope becomes closer to 0 and is less distinguishable from smoke. It is possible that due to the amount of SO_2 that
630 Raikoke injected into the stratosphere that the particles were substantially larger than particles from Ambae and Ulawun, thereby making them appear smoke-like within this classification scheme. While viable, this situation is not realistic if the particles are in fact as small as indicated using the Wrana et al. (2021) methodology.

 The second option is that smoke was in the stratosphere, but did not make up a large fraction of the total particle count and was below the detection threshold for observing the carbonyl stretch in the ACE-FTS residuals spectra. For example, the
635 maximum change in slope (relative to the background sulfuric acid slope) in Fig. 19 occurred at 16 km where the slope changed by 32%. Using the 70 nm background curves in Fig. 5 as a guide, we see that the amount of smoke required to shift the spectral slope by 32% ranged from 0.5% for pure BC to 0.9% for pure BrC. However, if the atmosphere was previously perturbed by a volcanic or wildfire event (i.e., the calculated background slopes were not representative of true background conditions) then

the 150 nm curves of Fig. 5 indicate that the amount of smoke required to shift the spectral slope by 32% ranged from 6% for pure BC to 35% for pure BrC. Because of the multiple assumptions that went into the creation of Fig. 5 we do not present these numbers as an estimate of the relative amount of smoke in the stratosphere at this time. However, what this indicates is how disproportionate the impact of smoke may be as compared to enhanced sulfuric acid aerosol as well as the importance of correctly characterizing the background statistics. Further, we saw no indication that the stratosphere was outside background conditions (i.e., no indication that sulfuric acid particles were larger than 70–90 nm). Therefore, it is possible, based on our simple theoretical model, that a smoke contribution of <1% may be responsible for the smoke classifications we saw in Figs. 16 and 17. We find this possibility to be interesting, and it would make an interesting future study that includes analysis of the ACE-FTS sensitivity to low mixing ratios of smoke.

8 Conclusions

We presented a method of distinguishing between sulfuric acid aerosol and smoke using the SAGE III/ISS extinction spectra. This methodology was evaluated using 4 case-study events (2 volcanic, 2 pyroCb) and using the CALIOP depolarization ratio and vertical feature mask. The CALIOP data were supportive of the smoke/sulfuric acid aerosol identification. The classification of the 2 volcanic events (Ambae and Ulawun eruptions) was nearly monolithic in correctly classifying the particles as sulfuric acid (i.e., >99.5% correct classification). Identification of aerosol source for the wildfire events was more challenging in that a non-negligible fraction of the spectra were incorrectly identified as sulfuric acid aerosol. Potential justifications for these misclassifications were presented. However, for the pyroCb events, the spectra with the largest k_{1020} and/or smallest slopes were uniformly identified as smoke yielding a correct classification rate of 81%.

While we cannot provide a clear definition of magnitude of event required for this method to be applicable, we can state two general cases where it is more likely to fail and the information provided within the introduction should allow the reader to put these events in their proper perspective. First, very small wildfire events may not inject enough smoke into the stratosphere to sufficiently change the slope spectral slope from background conditions. Similarly, even for large events, if the SAGE sample volume only contains optically thin smoke layers , this too would (e.g., viewing through thin filaments as opposed to through the plume's centroid), this too could lead to a sulfuric acid classification. In these cases, we note that classifying these layers as sulfuric acid is not necessarily wrong since the majority of these particles may be composed of background the particles within the sample volume are likely composed of sulfuric acid; this just fails to identify the presence of smoke (i.e., a "false negative" conclusion). Second, during large-scale volcanic eruptions (e.g., Pinatubo with VEI 6), there is a chance for a "false positive" in classifying the resultant sulfuric acid (possibly ash) particlesas smokethe probability for misclassifying the large sulfuric acid particles, or ash, as smoke is high. Under this scenario, massive amounts of ash and SO_2 is injected into the stratosphere, resulting in the formation of large sulfuric acid aerosol particles (e.g., > 500 nm). This would result in a spectrally flat extinction spectrum, which effectively mimics the behavior of smoke in the slope analysis. Usage of this method in either of these conditions is questionable. However, this method is applicable to all events within the SAGE III/ISS record to date with the possible exception being the Raikoke eruption, which must be interpreted carefully.

Interpreting spectra collected during mixed events, such as the combination of the Raikoke eruption and ~~NH~~ northern hemisphere pyroCb activity in 2019, presents ~~another~~ a challenging case. Ideally, we would understand the composition of these particles, which would provide better understanding for how they interact with light, and we may be able to better model the system. Indeed, in situ sampling of stratospheric smoke would prove valuable for improving this method as well as improving climate and chemistry models. However, with these limitations in mind, we presented a framework for interpreting data from mixed events that allows the reader to understand not only the assumptions herein, but the conditions under which conclusions are either reasonable or tenuous.

~~Finally, we demonstrated that the secondary plume that broke off from the main Raikoke plume and moved southward was composed primarily of smoke~~ We demonstrated that this technique classified the aerosol in the secondary Raikoke plume as predominantly smoke at higher altitudes (22–25 km) while the aerosol at lower altitudes ~~was~~ (14–21 km) was classified as predominantly sulfuric acid~~with a smaller contribution from smoke~~. This is supportive of the initial hypothesis that the secondary plume was composed of smoke and suggests that the smoke and sulfuric acid particles separated as they moved southward: smoke continued to loft to higher altitudes while sulfuric acid stayed at lower altitudes. ~~While these two aerosol types separated, they did not do so perfectly. Indeed, we identified traces of smoke in the lower altitudes and~~ These classifications require the caveat that, as discussed in §5.2, a smoke classification does not necessarily indicate that the observed aerosol layer was composed solely of smoke; rather, this indicates that smoke was present within this layer. Figure 5 was included to demonstrate the potential sensitivity the spectral slope may have to BC and BrC.

While these results supported the initial hypothesis, we also discussed the possible misclassification of sulfuric acid aerosol as smoke in the post-Raikoke stratosphere. The ACE-FTS products and spectra were used to identify the presence of smoke in the stratosphere between 20°N and 60°N. Indeed, smoke was identified within these latitudes and within the stratosphere using the ACE-FTS data, but the ACE-FTS data showed no spectral evidence of smoke above ≈20 km. The ACE-FTS team estimated sulfuric acid particle radii on the order of 200 nm, which was larger that what may be inferred from the SAGE data using the Wrana et al. (2021) technique. An alternative explanation that included the possibility of low-concentration smoke particles was also discussed. Per the model presented in Fig. 5, a relatively small amount of smoke (i.e., <1%) may significantly change the spectral slope as compared to background conditions. Because the method of identifying smoke in the ACE-FTS spectra (i.e., finding the carbonyl stretch) uses residuals, we question whether this feature would be visible in the spectra when <1% of the particles are smoke. While we find this possibility intriguing, it requires further investigation for support and we note that the radii estimated from ACE-FTS would yield spectral slopes comparable to the slopes presented in panel (a) of Fig. 19. Therefore, we conclude that it is reasonable that the aerosol layers we classified as smoke during the Raikoke time period were composed of larger sulfuric acid aerosol ~~at the higher altitudes. The general pattern we observed is that these species separated in a manner that is consistent with the expected behavior based on their refractive index values.~~ and we were unable to find definitive support for smoke at altitudes above 20 km.

One aspect we did not consider within this study was the possibility of mixed composition particles. As discussed above, recent studies (Ansmann et al., 2021; Magaritz-Ronen and Raveh-Rubin, 2021; Ohneiser et al., 2021) have hypothesized that smoke that comes from non-pyroCb fires have a longer residence time in the troposphere wherein these particles undergo

chemistry and adsorb water (presumably sulfuric acid as well) as they continue to loft to higher altitudes before eventually entering the stratosphere. If this is true, then these smoke particles would be significantly different from smoke particles that are injected directly into the stratosphere from pyroCb activity. These studies demonstrated that the aerosol layers they

710 identified as smoke exhibited different spectral behavior than what has been traditionally expected for smoke. While we can neither verify nor refute the conclusions of these studies, we find this to be an interesting possibility for future investigations. If these particles were coated with water or sulfuric acid and had a carbon core, then the question must be raised as to how this would impact the spectral slope analysis as well as the interpretation of the presence, or lack thereof, of the carbonyl smoke signature in the ACE-FTS data. Indeed, this merits further evaluation.

715 The stratosphere has provided many interesting and challenging puzzles during the Raikoke time period. Indeed, recent publications such as Ansmann et al. (2021), Magaritz-Ronen and Raveh-Rubin (2021), and Ohneiser et al. (2021) have challenged the accepted view of how smoke enters the stratosphere, how stratospheric smoke may be identified in lidar data, as well as the interpretation of CALIOP data. While their findings lend credence to our smoke classifications, they are contrary to what was observed in ACE-FTS. Therefore, at this point, the overall conclusions of the disparate analyses are incongruous and we view

720 this as an opportunity to either better understand the interpretation of our respective data sets or to better understand a previously unrealized aspect of the atmosphere (i.e., all of the research groups are right, but the results are seemingly incongruous because they are only seeing one piece of the puzzle). Indeed, the post-Raikoke stratosphere merits further detailed investigation to clarify these disparate conclusions and elucidate the corresponding chemistry, composition, and physics of these layers.

Data availability. The SAGE and CALIOP data used within this study are available on NASA's Atmospheric Science Data Center (https://eosweb.larc.nasa

725 the TropOMI data are available at the Copernicus Open Access Hub (https://scihub.copernicus.eu/), and ACE-FTS data are available from the ACE/SCISAT Database (https://databace.scisat.ca/).

Author contributions. TNK and LT developed the methodology, while TNK carried out the analysis, wrote the analysis code and the manuscript. RD, MK, DF, JT, and JK participated in scientific discussions and provided guidance throughout the study. JT and JK provided guidance on the use and interpretation of the CALIOP data. All authors reviewed the manuscript during the preparation process

730 *Competing interests.* The authors declare that they have no competing interests.

Acknowledgements. SAGE III/ISS is a NASA Langley managed mission funded by the NASA Science Mission Directorate within the Earth Systematic Mission Program. Enabling partners are the NASA Human Exploration and Operations Mission Directorate, International Space Station Program and the European Space Agency. SSAI personnel are supported through the STARSS III contract NNL16AA05C.

References

Alexander, D. T., Crozier, P. A., and Anderson, J. R.: Brown carbon spheres in East Asian outflow and their optical properties, Science, 321, 833–836, https://doi.org/10.1126/science.1155296, 2008.

Ansmann, A., Ohneiser, K., Chudnovsky, A., Baars, H., and Engelmann, R.: CALIPSO Aerosol-Typing Scheme Misclassified Stratospheric Fire Smoke: Case Study From the 2019 Siberian Wildfire Season, Frontiers in Environmental Science, 9, https://doi.org/10.3389/fenvs.2021.769852, 2021.

Bachmeier, Scott: PyroCb in Russia, http://pyrocb.ssec.wisc.edu/archives/2321, accessed: 2021-02-23, 2019.

Bergstrom, R. W., Russell, P. B., and Hignett, P.: Wavelength Dependence of the Absorption of Black Carbon Particles: Predictions and Results from the TARFOX Experiment and Implications for the Aerosol Single Scattering Albedo, Journal of the Atmospheric Sciences, 59, 567–577, https://doi.org/10.1175/1520-0469(2002)059<0567:WDOTAO>2.0.CO;2, 2002.

Bernath, P. F., McElroy, C. T., Abrams, M. C., Boone, C. D., Butler, M., Camy-Peyret, C., Carleer, M., Clerbaux, C., Coheur, P.-F., Colin, R., DeCola, P., DeMazière, M., Drummond, J. R., Dufour, D., Evans, W. F. J., Fast, H., Fussen, D., Gilbert, K., Jennings, D. E., Llewellyn, E. J., Lowe, R. P., Mahieu, E., McConnell, J. C., McHugh, M., McLeod, S. D., Michaud, R., Midwinter, C., Nassar, R., Nichitiu, F., Nowlan, C., Rinsland, C. P., Rochon, Y. J., Rowlands, N., Semeniuk, K., Simon, P., Skelton, R., Sloan, J. J., Soucy, M.-A., Strong, K., Tremblay, P., Turnbull, D., Walker, K. A., Walkty, I., Wardle, D. A., Wehrle, V., Zander, R., and Zou, J.: Atmospheric Chemistry Experiment (ACE): Mission overview, Geophysical Research Letters, 32, L15S01, https://doi.org/10.1029/2005GL022386, 2005.

Bluth, G. J. S., Doiron, S. D., Schnetzler, C. C., Krueger, A. J., and Walter, L. S.: Global tracking of the SO2 clouds from the June, 1991 Mount Pinatubo eruptions, Geophysical Research Letters, 19, 151–154, https://doi.org/10.1029/91GL02792, 1992.

Boers, R., de Laat, A. T., Stein Zweers, D. C., and Dirksen, R. J.: Lifting potential of solar-heated aerosol layers, Geophysical Research Letters, 37, L24 802, https://doi.org/10.1029/2010GL045171, 2010.

Boone, C. D., Nassar, R., Walker, K. A., Rochon, Y., McLeod, S. D., Rinsland, C. P., and Bernath, P. F.: Retrievals for the atmospheric chemistry experiment Fourier-transform spectrometer, Applied Optics, 44, 7218–7231, https://doi.org/10.1364/AO.44.007218, 2005.

Boone, C. D., Bernath, P. F., and Fromm, M. D.: Pyrocumulonimbus Stratospheric Plume Injections Measured by the ACE-FTS, Geophysical Research Letters, 47, e2020GL088 442, https://doi.org/10.1029/2020GL088442, e2020GL088442 2020GL088442,, 2020.

Chagnon, C. and Junge, C.: The Vertical Distribution of Sub-Micron Particles in the Stratosphere, Journal of Meteorology, 18, 746–752, https://doi.org/10.1175/1520-0469(1961)018<0746:TVDOSM>2.0.CO;2, 1961.

Chakrabarty, R. K., Moosmüller, H., Chen, L.-W. A., Lewis, K., Arnott, W. P., Mazzoleni, C., Dubey, M. K., Wold, C. E., Hao, W. M., and Kreidenweis, S. M.: Brown carbon in tar balls from smoldering biomass combustion, Atmospheric Chemistry and Physics, 10, 6363–6370, https://doi.org/10.5194/acp-10-6363-2010, 2010.

Chouza, F., Leblanc, T., Barnes, J., Brewer, M., Wang, P., and Koon, D.: Long-term (1999–2019) variability of stratospheric aerosol over Mauna Loa, Hawaii, as seen by two co-located lidars and satellite measurements, Atmospheric Chemistry and Physics, 20, 6821–6839, https://doi.org/10.5194/acp-20-6821-2020, 2020.

Christian, K., Yorks, J., and Das, S.: Differences in the Evolution of Pyrocumulonimbus and Volcanic Stratospheric Plumes as Observed by CATS and CALIOP Space-Based Lidars, Atmosphere, 11, https://doi.org/10.3390/atmos11101035, 2020.

Cisewski, M., Zawodny, J., Gasbarre, J., Eckman, R., Topiwala, N., Rodriguez-Alvarez, O., Cheek, D., and Hall, S.: The Stratospheric Aerosol and Gas Experiment (SAGE III) on the International Space Station (ISS) Mission, in: Sensors, Systems, and Next-Generation Satellites XVIII, edited by Meynart, R and Neeck, SP and Shimoda, H, vol. 9241 of *Proceedings of SPIE*, p. 924107, SPIE,

https://doi.org/10.1117/12.2073131, Conference on Sensors, Systems, and Next-Generation Satellites XVIII, Amsterdam, Netherlands, Sep 22-25, 2014, 2014.

D'Arrigo, R., Seager, R., Smerdon, J. E., LeGrande, A. N., and Cook, E. R.: The anomalous winter of 1783–1784: Was the Laki eruption or an analog of the 2009–2010 winter to blame?, Geophysical Research Letters, 38, L05 706, https://doi.org/10.1029/2011GL046696, 2011.

de Laat, A. T. J., Stein Zweers, D. C., Boers, R., and Tuinder, O. N. E.: A solar escalator: Observational evidence of the self-lifting of smoke and aerosols by absorption of solar radiation in the February 2009 Australian Black Saturday plume, Journal of Geophysical Research: Atmospheres, 117, D04 204, https://doi.org/10.1029/2011JD017016, 2012.

de Leeuw, J., Schmidt, A., Witham, C. S., Theys, N., Taylor, I. A., Grainger, R. G., Pope, R. J., Haywood, J., Osborne, M., and Kristiansen, N. I.: The 2019 Raikoke volcanic eruption: Part 1 Dispersion model simulations and satellite retrievals of volcanic sulfur dioxide, Atmospheric Chemistry and Physics Discussions, 2020, 1–38, https://doi.org/10.5194/acp-2020-889, 2020.

de Leeuw, J., Schmidt, A., Witham, C. S., Theys, N., Taylor, I. A., Grainger, R. G., Pope, R. J., Haywood, J., Osborne, M., and Kristiansen, N. I.: The 2019 Raikoke volcanic eruption – Part 1: Dispersion model simulations and satellite retrievals of volcanic sulfur dioxide, Atmospheric Chemistry and Physics, 21, 10 851–10 879, https://doi.org/10.5194/acp-21-10851-2021, 2021.

Deshler, T., Hervig, M., Hofmann, D., Rosen, J., and Liley, J.: Thirty years of in situ stratospheric aerosol size distribution measurements from Laramie, Wyoming (41°N), using balloon-borne instruments, Journal of Geophysical Research-Atmospheres, 108, 4167, https://doi.org/10.1029/2002JD002514, 2003.

Forrister, H., Liu, J., Scheuer, E., Dibb, J., Ziemba, L., Thornhill, K. L., Anderson, B., Diskin, G., Perring, A. E., Schwarz, J. P., et al.: Evolution of brown carbon in wildfire plumes, Geophysical Research Letters, 42, 4623–4630, https://doi.org/10.1002/2015GL063897, 2015.

Fromm, M., Tupper, A., Rosenfeld, D., Servranckx, R., and McRae, R.: Violent pyro-convective storm devastates Australia's capital and pollutes the stratosphere, Geophysical Research Letters, 33, L05 815, https://doi.org/10.1029/2005GL025161, 2006.

Fromm, M., Lindsey, D. T., Servranckx, R., Yue, G., Trickl, T., Sica, R., Doucet, P., and Godin-Beekmann, S.: The Untold Story of Pyrocumulonimbus, Bulletin of the American Meteorological Society, 91, 1193–1210, https://doi.org/10.1175/2010BAMS3004.1, 2010.

Getzewich, B. J., Vaughan, M. A., Hunt, W. H., Avery, M. A., Powell, K. A., Tackett, J. L., Winker, D. M., Kar, J., Lee, K.-P., and Toth, T. D.: CALIPSO lidar calibration at 532 nm: version 4 daytime algorithm, Atmospheric Measurement Techniques, 11, 6309–6326, https://doi.org/10.5194/amt-11-6309-2018, 2018.

Gorkavyi, N., Krotkov, N., Li, C., Lait, L., Colarco, P., Carn, S., DeLand, M., Newman, P., Schoeberl, M., Taha, G., Torres, O., Vasilkov, A., and Joiner, J.: Tracking aerosols and SO_2 clouds from the Raikoke eruption: 3D view from satellite observations, Atmospheric Measurement Techniques, 14, 7545–7563, https://doi.org/10.5194/amt-14-7545-2021, 2021.

Hedelt, P., Efremenko, D. S., Loyola, D. G., Spurr, R., and Clarisse, L.: Sulfur dioxide layer height retrieval from Sentinel-5 Precursor/TROPOMI using FP_ILM, Atmospheric Measurement Techniques, 12, 5503–5517, https://doi.org/10.5194/amt-12-5503-2019, 2019.

Johnson, M. S., Strawbridge, K., Knowland, K. E., Keller, C., and Travis, M.: Long-range transport of Siberian biomass burning emissions to North America during FIREX-AQ, Atmospheric Environment, 252, 118 241, https://doi.org/10.1016/j.atmosenv.2021.118241, 2021.

Johnston, F. H., Borchers-Arriagada, N., Morgan, G. G., Jalaludin, B., Palmer, A. J., Williamson, G. J., and Bowman, D. M. J. S.: Unprecedented health costs of smoke-related PM2.5 from the 2019-20 Australian megafires, Nature Sustainability, 4, 42–47, https://doi.org/10.1038/s41893-020-00610-5, 2020.

Kablick III, G. P., Allen, D. R., Fromm, M. D., and Nedoluha, G. E.: Australian PyroCb Smoke Generates Synoptic-Scale Stratospheric Anticyclones, Geophysical Research Letters, 47, e2020GL088 101, https://doi.org/10.1029/2020GL088101, 2020.

Kar, J., Vaughan, M. A., Kam-Pui, L., Tackett, J. L., Avery, M. A., Garnier, A., Getzewich, B. J., Hunt, W. H., Josset, D., Liu, Z., et al.: CALIPSO lidar calibration at 532 nm: version 4 nighttime algorithm, Atmospheric Measurement Techniques, 11, 1459–1479, https://doi.org/10.5194/amt-11-1459-2018, 2018.

Kar, J., Lee, K.-P., Vaughan, M. A., Tackett, J. L., Trepte, C. R., Winker, D. M., Lucker, P. L., and Getzewich, B. J.: CALIPSO level 3 stratospheric aerosol profile product: version 1.00 algorithm description and initial assessment, Atmospheric Measurement Techniques, 12, 6173–6191, https://doi.org/10.5194/amt-12-6173-2019, 2019.

Kim, M.-H., Omar, A. H., Tackett, J. L., Vaughan, M. A., Winker, D. M., Trepte, C. R., Hu, Y., Liu, Z., Poole, L. R., Pitts, M. C., Kar, J., and Magill, B. E.: The CALIPSO version 4 automated aerosol classification and lidar ratio selection algorithm, Atmospheric Measurement Techniques, 11, 6107–6135, https://doi.org/10.5194/amt-11-6107-2018, 2018.

Kirchstetter, T. W., Novakov, T., and Hobbs, P. V.: Evidence that the spectral dependence of light absorption by aerosols is affected by organic carbon, Journal of Geophysical Research: Atmospheres, 109, https://doi.org/10.1029/2004JD004999, 2004.

Kloss, C., Berthet, G., Sellitto, P., Ploeger, F., Taha, G., Tidiga, M., Eremenko, M., Bossolasco, A., Jégou, F., Renard, J.-B., and Legras, B.: Stratospheric aerosol layer perturbation caused by the 2019 Raikoke and Ulawun eruptions and their radiative forcing, Atmospheric Chemistry and Physics, 21, 535–560, https://doi.org/10.5194/acp-21-535-2021, 2021.

Knepp, T. N., Thomason, L., Roell, M., Damadeo, R., Leavor, K., Leblanc, T., Chouza, F., Khaykin, S., Godin-Beekmann, S., and Flittner, D.: Evaluation of a Method for Converting SAGE Extinction Coefficients to Backscatter Coefficient for Intercomparison with LIDAR Observations, Atmospheric Measurement Techniques Discussions, 2020, 1–24, https://doi.org/10.5194/amt-2020-60, 2020.

Kozlov, V. S., Yausheva, E. P., Terpugova, S. A., Panchenko, M. V., Chernov, D. G., and Shmargunov, V. P.: Optical–microphysical properties of smoke haze from Siberian forest fires in summer 2012, International Journal of Remote Sensing, 35, 5722–5741, https://doi.org/10.1080/01431161.2014.945010, 2014.

Kremser, S., Thomason, L. W., von Hobe, M., Hermann, M., Deshler, T., Timmreck, C., Toohey, M., Stenke, A., Schwarz, J. P., Weigel, R., Fueglistaler, S., Prata, F. J., Vernier, J.-P., Schlager, H., Barnes, J. E., Antuna-Marrero, J.-C., Fairlie, D., Palm, M., Mahieu, E., Notholt, J., Rex, M., Bingen, C., Vanhellemont, F., Bourassa, A., Plane, J. M. C., Klocke, D., Carn, S. A., Clarisse, L., Trickl, T., Neely, R., James, A. D., Rieger, L., Wilson, J. C., and Meland, B.: Stratospheric aerosol-Observations, processes, and impact on climate, Reviews of Geophysics, 54, 278–335, https://doi.org/10.1002/2015RG000511, 2016.

Leys, C., Ley, C., Klein, O., Bernard, P., and Licata, L.: Detecting outliers: Do not use standard deviation around the mean, use absolute deviation around the median, Journal of Experimental Social Psychology, 49, 764–766, https://doi.org/10.1016/j.jesp.2013.03.013, 2013.

Liu, P. F., Abdelmalki, N., Hung, H.-M., Wang, Y., Brune, W. H., and Martin, S. T.: Ultraviolet and visible complex refractive indices of secondary organic material produced by photooxidation of the aromatic compounds toluene and m-xylene, Atmospheric Chemistry and Physics, 15, 1435–1446, https://doi.org/10.5194/acp-15-1435-2015, 2015.

Magaritz-Ronen, L. and Raveh-Rubin, S.: Wildfire Smoke Highlights Troposphere-to-Stratosphere Pathway, Geophysical Research Letters, 48, e2021GL095 848, https://doi.org/10.1029/2021GL095848, e2021GL095848 2021GL095848, 2021.

McCormick, M., Thomason, L., and Trepte, C.: Atmospheric Effects of the Mt-Pinatubo Eruption, Nature, 373, 399–404, https://doi.org/10.1038/373399a0, 1995.

Moore, R. H., Wiggins, E. B., Ahern, A. T., Zimmerman, S., Montgomery, L., Campuzano Jost, P., Robinson, C. E., Ziemba, L. D., Winstead, E. L., Anderson, B. E., Brock, C. A., Brown, M. D., Chen, G., Crosbie, E. C., Guo, H., Jimenez, J. L., Jordan, C. E., Lyu, M., Nault, B. A., Rothfuss, N. E., Sanchez, K. J., Schueneman, M., Shingler, T. J., Shook, M. A., Thornhill, K. L., Wagner, N. L., and Wang, J.: Sizing response of the Ultra-High Sensitivity Aerosol Spectrometer (UHSAS) and Laser Aerosol Spectrometer (LAS) to changes in submicron

aerosol composition and refractive index, Atmospheric Measurement Techniques, 14, 4517–4542, https://doi.org/10.5194/amt-14-4517-2021, 2021.

Müller, D., Mattis, I., Wandinger, U., Ansmann, A., Althausen, D., and Stohl, A.: Raman lidar observations of aged Siberian and Canadian forest fire smoke in the free troposphere over Germany in 2003: Microphysical particle characterization, Journal of Geophysical Research: Atmospheres, 110, D17 201, https://doi.org/10.1029/2004JD005756, 2005.

Murphy, D., Thomson, D., and Mahoney, T.: In situ measurements of organics, meteoritic material, mercury, and other elements in aerosols at 5 to 19 kilometers, Science, 282, 1664–1669, https://doi.org/10.1126/science.282.5394.1664, 1998.

Muser, L. O., Hoshyaripour, G. A., Bruckert, J., Horvath, A., Malinina, E., Peglow, S., Prata, F. J., Rozanov, A., von Savigny, C., Vogel, H., and Vogel, B.: Particle Aging and Aerosol–Radiation Interaction Affect Volcanic Plume Dispersion: Evidence from Raikoke Eruption 2019, Atmospheric Chemistry and Physics Discussions, 2020, 1–27, https://doi.org/10.5194/acp-2020-370, 2020.

Newhall, C. G. and Self, S.: The volcanic explosivity index (VEI) an estimate of explosive magnitude for historical volcanism, Journal of Geophysical Research: Oceans, 87, 1231–1238, https://doi.org/10.1029/JC087iC02p01231, 1982.

Ohneiser, K., Ansmann, A., Chudnovsky, A., Engelmann, R., Ritter, C., Veselovskii, I., Baars, H., Gebauer, H., Griesche, H., Radenz, M., Hofer, J., Althausen, D., Dahlke, S., and Maturilli, M.: The unexpected smoke layer in the High Arctic winter stratosphere during MOSAiC 2019–2020, Atmospheric Chemistry and Physics, 21, 15 783–15 808, https://doi.org/10.5194/acp-21-15783-2021, 2021.

Osborne, M. J., de Leeuw, J., Witham, C., Schmidt, A., Beckett, F., Kristiansen, N., Buxmann, J., Saint, C., Welton, E. J., Fochesatto, J., Gomes, A. R., Bundke, U., Petzold, A., Marenco, F., and Haywood, J.: The 2019 Raikoke volcanic eruption part 2: Particle phase dispersion and concurrent wildfire smoke emissions, Atmospheric Chemistry and Physics Discussions, 2021, 1–36, https://doi.org/10.5194/acp-2021-448, 2021.

Palmer, K. and Williams, D.: Optical-Constants of Sulfuric-Acid - Application to Clouds of Venus, Applied Optics, 14, 208–219, https://doi.org/10.1364/AO.14.000208, 1975.

Park, Y. H., Sokolik, I. N., and Hall, S. R.: The impact of smoke on the ultraviolet and visible radiative forcing under different fire regimes, Air, Soil and Water Research, 11, 1–10, https://doi.org/10.1177/1178622118774803, 2018.

Peterson, D., R. Campbell, J., Hyer, E., D. Fromm, M., P. Kablick, G., H. Cossuth, J., and Deland, M.: Wildfire-driven thunderstorms cause a volcano-like stratospheric injection of smoke, npj Climate and Atmospheric Science, 1, , https://doi.org/10.1038/s41612-018-0039-3, 2018.

Pinto, J. P., Turco, R. P., and Toon, O. B.: Self-limiting physical and chemical effects in volcanic eruption clouds, Journal of Geophysical Research: Atmospheres, 94, 11 165–11 174, https://doi.org/10.1029/JD094iD08p11165, 1989.

Pitts, M. and Thomason, L.: The Impact of the Eruptions of Mount-Pinatubo and Cerro Hudson on Antarctic Aerosol Levels During the 1991 Austral Spring, Geophysical Research Letters, 20, 2451–2454, https://doi.org/10.1029/93GL02160, 1993.

Prata, A. T., Young, S. A., Siems, S. T., and Manton, M. J.: Lidar ratios of stratospheric volcanic ash and sulfate aerosols retrieved from CALIOP measurements, Atmospheric Chemistry and Physics, 17, 8599–8618, https://doi.org/10.5194/acp-17-8599-2017, 2017.

Pyle, D. M.: Mass and energy budgets of explosive volcanic eruptions, Geophysical Research Letters, 22, 563–566, https://doi.org/10.1029/95GL00052, 1995.

Rashidov, V., Girina, O., Ozerov, A. Y., and Pavlov, N.: The June 2019. Eruption of Raikoke volcano (the Kurile Islands), Bulletin of Kamchatka Regional Association "Educational-Scientific Center". Earth Sciences, 42, 5–8, 2019.

Santer, B. D., Bonfils, C., Painter, J. F., Zelinka, M. D., Mears, C., Solomon, S., Schmidt, G. A., Fyfe, J. C., Cole, J. N., Nazarenko, L., et al.: Volcanic contribution to decadal changes in tropospheric temperature, Nature Geoscience, 7, 185–189, https://doi.org/10.1038/NGEO2098, 2014.

Schurer, A. P., Hegerl, G. C., Luterbacher, J., Brönnimann, S., Cowan, T., Tett, S. F. B., Zanchettin, D., and Timmreck, C.: Disentangling the causes of the 1816 European year without a summer, Environmental Research Letters, 14, 094 019, https://doi.org/10.1088/1748-9326/ab3a10, 2019.

Stothers, R. B.: The Great Tambora Eruption in 1815 and Its Aftermath, Science, 224, 1191–1198, https://doi.org/10.1126/science.224.4654.1191, 1984.

Sumlin, B. J., Heinson, Y. W., Shetty, N., Pandey, A., Pattison, R. S., Baker, S., Hao, W. M., and Chakrabarty, R. K.: UV–Vis–IR spectral complex refractive indices and optical properties of brown carbon aerosol from biomass burning, Journal of Quantitative Spectroscopy and Radiative Transfer, 206, 392–398, https://doi.org/https://doi.org/10.1016/j.jqsrt.2017.12.009, 2018.

Tanakadate, H.: The volcanic activity of Japan during 1914-1924, Bulletin Volcanologique, 1, 3–19, https://doi.org/10.1007/BF02719558, 1925.

Tereszchuk, K. A., González Abad, G., Clerbaux, C., Hadji-Lazaro, J., Hurtmans, D., Coheur, P.-F., and Bernath, P. F.: ACE-FTS observations of pyrogenic trace species in boreal biomass burning plumes during BORTAS, Atmospheric Chemistry and Physics, 13, 4529–4541, https://doi.org/10.5194/acp-13-4529-2013, 2013.

Theys, N., De Smedt, I., Yu, H., Danckaert, T., van Gent, J., Hörmann, C., Wagner, T., Hedelt, P., Bauer, H., Romahn, F., Pedergnana, M., Loyola, D., and Van Roozendael, M.: Sulfur dioxide retrievals from TROPOMI onboard Sentinel-5 Precursor: algorithm theoretical basis, Atmospheric Measurement Techniques, 10, 119–153, https://doi.org/10.5194/amt-10-119-2017, 2017.

Thomason, L.: Observations of a New SAGE-II Aerosol Extinction Mode Following the Eruption of Mt-Pinatubo, Geophysical Research Letters, 19, 2179–2182, https://doi.org/10.1029/92GL02185, 1992.

Thomason, L. W., Kovilakam, M., Schmidt, A., von Savigny, C., Knepp, T., and Rieger, L.: Evidence for the predictability of changes in the stratospheric aerosol size following volcanic eruptions of diverse magnitudes using space-based instruments, Atmospheric Chemistry and Physics, 21, 1143–1158, https://doi.org/10.5194/acp-21-1143-2021, 2021.

Thomason, L. W., Burton, S. P., Luo, B. P., and Peter, T.: SAGE II measurements of stratospheric aerosol properties at non-volcanic levels, Atmospheric Chemistry and Physics, 8, 983–995, https://doi.org/10.5194/acp-8-983-2008, 2008.

Thordarson, T. and Self, S.: The Laki (Skaftár Fires) and Grímsvötn eruptions in 1783–1785, Bulletin of Volcanology, 55, 233–263, 1993.

Thordarson, T. and Self, S.: Atmospheric and environmental effects of the 1783–1784 Laki eruption: A review and reassessment, Journal of Geophysical Research: Atmospheres, 108, AAC 7–1–AAC 7–29, https://doi.org/10.1029/2001JD002042, 2003.

Turco, R. P., Toon, O. B., Ackerman, T. P., Pollack, J. B., and Sagan, C.: Nuclear winter: Global consequences of multple nuclear explosions, Science, 222, 1283–1292, 1983.

Vaughan, G., Wareing, D., and Ricketts, H.: Measurement Report: Lidar measurements of stratospheric aerosol following the 2019 Raikoke and Ulawun volcanic eruptions, Atmospheric Chemistry and Physics, 21, 5597–5604, https://doi.org/10.5194/acp-21-5597-2021, 2021.

Vaughan, M., Pitts, M., Trepte, C., Winker, D., Detweiler, P., Garnier, A., Getzewich, B., Hunt, W., Lambeth, J., Lee, K.-P., Lucker, P., Murray, T., Rodier, S., Tremas, T., Bazureau, A., and Pelon, J.: Cloud –Aerosol LIDAR Infrared Pathfinder Satellite Observations: Data Management System, Data Products Catalog, Release 4.30, Report, National Aeronautics and Space Administration, accessed: 2021-05-27, 2018.

920 Vaughan, M. A., Powell, K. A., Winker, D. M., Hostetler, C. A., Kuehn, R. E., Hunt, W. H., Getzewich, B. J., Young, S. A., Liu, Z., and McGill, M. J.: Fully Automated Detection of Cloud and Aerosol Layers in the CALIPSO Lidar Measurements, Journal of Atmospheric and Oceanic Technology, 26, 2034–2050, https://doi.org/10.1175/2009JTECHA1228.1, 2009.

Veefkind, J., Aben, I., McMullan, K., Förster, H., de Vries, J., Otter, G., Claas, J., Eskes, H., de Haan, J., Kleipool, Q., van Weele, M., Hasekamp, O., Hoogeveen, R., Landgraf, J., Snel, R., Tol, P., Ingmann, P., Voors, R., Kruizinga, B., Vink, R., Visser, H., and Levelt, P.:
925 TROPOMI on the ESA Sentinel-5 Precursor: A GMES mission for global observations of the atmospheric composition for climate, air quality and ozone layer applications, Remote Sensing of Environment, 120, 70–83, https://doi.org/10.1016/j.rse.2011.09.027, 2012.

Vernier, J. P., Thomason, L. W., Pommereau, J. P., Bourassa, A., Pelon, J., Garnier, A., Hauchecorne, A., Blanot, L., Trepte, C., Degenstein, D., and Vargas, F.: Major influence of tropical volcanic eruptions on the stratospheric aerosol layer during the last decade, Geophysical Research Letters, 38, L12 807, https://doi.org/10.1029/2011GL047563, 2011.

930 Wang, H. J. R., Damadeo, R., Flittner, D., Kramarova, N., Taha, G., Davis, S., Thompson, A. M., Strahan, S., Wang, Y., Froidevaux, L., Degenstein, D., Bourassa, A., Steinbrecht, W., Walker, K. A., Querel, R., Leblanc, T., Godin-Beekmann, S., Hurst, D., and Hall, E.: Validation of SAGE III/ISS Solar Occultation Ozone Products With Correlative Satellite and Ground-Based Measurements, Journal of Geophysical Research: Atmospheres, 125, e2020JD032 430, https://doi.org/10.1029/2020JD032430, e2020JD032430 2020JD032430, 2020.

935 Wilka, C., Shah, K., Stone, K., Solomon, S., Kinnison, D., Mills, M., Schmidt, A., and Neely, III, R. R.: On the Role of Heterogeneous Chemistry in Ozone Depletion and Recovery, Geophysical Research Letters, 45, 7835–7842, https://doi.org/10.1029/2018GL078596, 2018.

Winker, D., Pelon, J., Coakley Jr, J., Ackerman, S., Charlson, R., Colarco, P., Flamant, P., Fu, Q., Hoff, R., Kittaka, C., et al.: The CALIPSO mission: A global 3D view of aerosols and clouds, Bulletin of the American Meteorological Society, 91, 1211–1230,
940 https://doi.org/10.1175/2010BAMS3009.1, 2010.

Witham, C. S. and Oppenheimer, C.: Mortality in England during the 1783–4 Laki Craters eruption, Bulletin of Volcanology, 67, 15–26, 2004.

Womack, C. C., Manfred, K. M., Wagner, N. L., Adler, G., Franchin, A., Lamb, K. D., Middlebrook, A. M., Schwarz, J. P., Brock, C. A., Brown, S. S., and Washenfelder, R. A.: Complex refractive indices in the ultraviolet and visible spectral region for highly absorbing
945 non-spherical biomass burning aerosol, Atmospheric Chemistry and Physics, 21, 7235–7252, https://doi.org/10.5194/acp-21-7235-2021, 2021.

Wrana, F., von Savigny, C., Zalach, J., and Thomason, L. W.: Retrieval of stratospheric aerosol size distribution parameters using satellite solar occultation measurements at three wavelengths, Atmospheric Measurement Techniques, 14, 2345–2357, https://doi.org/10.5194/amt-14-2345-2021, 2021.

950 Yu, P., Toon, O., Bardeen, C., Zhu, Y., Rosenlof, K., Portmann, R., Thornberry, T., Gao, R.-S., Davis, S., Wolf, E., de Gouw, J., Peterson, D., Fromm, M., and Robock, A.: Black carbon lofts wildfire smoke high into the stratosphere to form a persistent plume, Science, 365, 587–590, https://doi.org/10.1126/science.aax1748, 2019.